ORIGINAL PAPER

Numerical Study on the Field-Scale Criterion of Hydraulic Fracture Crossing the Interface Between Roof and Broken Low-Permeability Coal

Hao Li[1] · Weiguo Liang[1,2] · Yulong Jiang[1,2] · Pengfei Wu[2] · Jianjun Wu[3] · Wei He[1,2]

Abstract

In areas of broken soft and low-permeability coal, indirect hydraulic fracturing (HF) coal is a technology with great potential to increase coal bed methane (CBM) production. The key to success of the technology is that HFs can cross the coal–rock interface from the roof and propagate into the coal. To this end, this article focuses on the roots that hinder the HFs propagating enough in the coal, that is, the significant inelastic deformation and abundant discontinuities of the coal. Based on CT experiments and nonlinear mechanics-seepage theory, a 3D discontinuities network model and plastic-nonlinear fracture-seepage coupled constitutive equations were established, respectively. On this basis, 115 numerical calculation models were established to study the field-scale criterion of HFs crossing coal–rock interface under the influence of three factors, including the distance between horizontal well and interface (D_{op}), interface friction coefficient ($f_{c,i}$) and in-situ stress difference ($\Delta\sigma$). The results show that the critical $f_{c,i}$ is positively correlated with D_{op} and negatively correlated with $\Delta\sigma$. Once the D_{op} exceeds 2 m, more than 80% of the hydraulic energy will be consumed in the nonlinear mechanical behavior and mixed fracture mode of coal, which will lead to the difficulty of HFs propagation. In-situ experiments show that, by reducing D_{op}, optimizing the landing of the horizontal well (i.e. increasing $\Delta\sigma$ and $f_{c,i}$), and maintaining high hydraulic energy (or injection rate), the daily CBM production by indirect fracturing technology is 10 times higher than that without parameter optimization, exceeding 3000m³/d. The "field-scale criterion" obtained in this article will provide theoretical support for increasing the success rate of indirect fracturing coal technology in areas of broken low-permeability coal.

Keywords Field-scale criterion · Hydraulic fracture · Coal-rock interface · Broken and low-permeability coal · Constitutive equations · Discontinuities network model

1 Introduction

The ultra-low permeability of coal beds often demands effective stimulation by hydraulic fracturing (HF) treatments, to produce coal bed methane (CBM) economically (Keshavarz et al. 2016; Sampath et al. 2017). Through the technology

of direct fracturing coal (Fig. 1b), that is, multi-stage HFs of horizontal well in coal bed, San Juan basin in the United States and Bowen basin in Australia have achieved high production of CBM (Thakur 2017). However, the successful experiences are difficult to be replicated in China. Compared with the primary structural coal in the United States and Australia, most of the coal bed in China is characterized by broken, soft (uniaxial compressive strength usually less than 15 MPa) and extremely low permeability (usually less than 1 mD) after a long-term and large-scale geological movement (Wang et al. 2015; Liu et al. 2017). The significant plastic deformation and nonlinear fracture characteristics of the coal will cause a large amount of hydraulic energy to be used to consume plastic work, rather than fracture surface energy which contributes to the HFs propagation. In addition, the abundant discontinuities of the coal cause HFs deflection and form a more energy-consuming mixed

✉ Hao Li
haolityut@163.com

1 Key Laboratory of In-Situ Property Improving Mining
   of Ministry of Education, Taiyuan University of Technology,
   Taiyuan 030024, China

2 College of Mining Engineering, Taiyuan University
   of Technology, Taiyuan 030024, China

3 Shanxi China Coal Huajin Energy Limited Liability
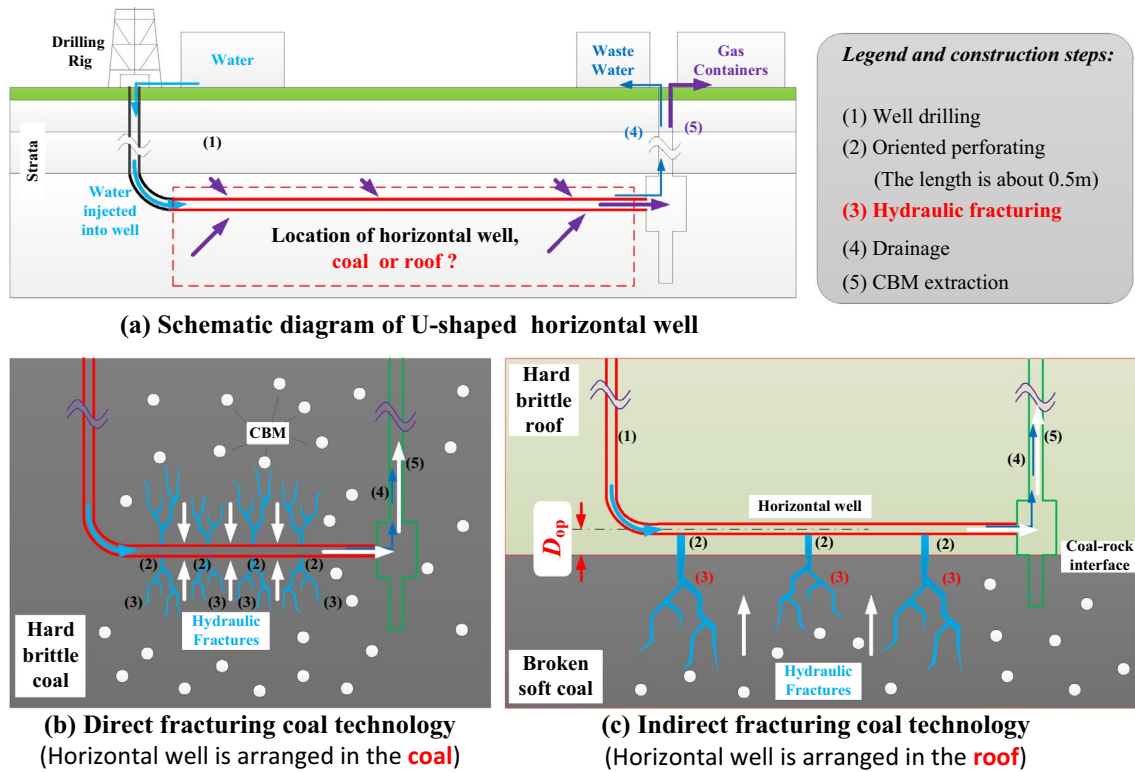   Company, Hejin 043300, Shanxi, China

(a) Schematic diagram of U-shaped horizontal well

(b) Direct fracturing coal technology
(Horizontal well is arranged in the **coal**)

(c) Indirect fracturing coal technology
(Horizontal well is arranged in the **roof**)

Fig. 1 Schematic diagram of two hydraulic fracturing technologies

fracture mode. As a result, the horizontal well in this poor medium is easy to collapse, and the HFs are short (Li et al. 2015; Zhang et al. 2018). Obviously, the conventional technology of "direct fracturing coal" is not suitable for the above abominable coal geology. On the contrary, if the horizontal well is arranged in the hard brittle roof instead of the broken soft coal, and then HFs propagate in rock and coal (i.e. "indirect fracturing coal" proposed by Olsen et al. 2007, as shown in Fig. 1c), the above problems can be avoided. The key to this unconventional technology is that the HFs can cross the interface between roof and broken low-permeability coal in field-scale.

Compared with laboratory tests and theoretical analysis, numerical simulation is a low-cost and efficient method to obtain the field-scale criterion of HFs crossing the interface between roof and the coal under the influence of multiple factors. However, reasonable numerical simulation results of hydraulic fracturing strongly depend on the solution of two core issues (Poludasu et al. 2016): (1) fluid–solid coupling constitutive equations, especially the nonlinear fracture mechanics equations applicable to the coal; (2) Three-dimensional geometric model of the coal discontinuities. For the first issue, many scholars have studied the HFs propagation in layered brittle rocks based on the theory of linear elastic fracture mechanics. Taking donnybrook sandstone or gas shale as the research objects, Llanos et al.

(2017) and Aimene et al. (2019) obtained results through experimental and theoretical analysis, that is, the maximum principal stress and discontinuity are the main reasons that affect the HFs cross the interface of the two media, rather than the friction coefficient. Jiang et al. (2016) and Huang et al. (2017) used numerical simulation method to sum up the critical stress differences and elastic modulus of brittle layered rocks when the HFs cross the interface, and found that interfaces can create mechanical interference, blunting the stress intensity at the crack tip and causing termination, especially under the condition of low stress anisotropy and high contrast between two layers. Based on the theory of linear elastic fracture mechanics, the extended finite element and phase field numerical calculation programs for hydraulic fracturing problem were established by Vahab et al. (2017) and Zhuang et al. (2019) respectively, the results showed that in general for stiff to soft configurations of material interfaces the probability of hydro-fracture penetration was quite high. Based on the calculation model of an infinite isotropic elastic medium with a planar crack, Kanaun (2018) established the finite element numerical calculation program of pure type I fracture in the process of hydraulic fracturing, and obtained the result that the fracture radius increased with the increase of water injection time and water injection pressure. In addition, some scholars used cohesive zone model based on elastic damage theory to simulate the

nonlinear fracture process of rock. Guo et al. (2017), Lan and Gong (2020) used the model to study the propagation law of HFs in layered shale. Numerical simulation results illustrated that HFs needed much more energy to cross the interface under a situation of high vertical stress and barrier tensile strength, thus, wide and long bi-wing normal fractures were likely to be generated. The second issue is also the focus of scholars, because the abundant discontinuities can induce HFs deflection and form more energy-consuming mixed or even shear fracture modes. There are several methods for numerical modeling of the discontinuities networks, including (1) Equivalent continuum model (ECM) (Hao et al. 2013), (2) Dual continuum model (DCM) (Moinfar et al. 2013; Sakhaee-Pour and Wheeler 2016) and (3) Discrete fracture network (DFN) (Karimpouli et al. 2017; Yu et al. 2019). Among them, DFN is favored because of its stochastic fracture network and the connectivity of large-scale discontinuities, thus the uncertainty can be quantified consequently (Karimpouli et al. 2017). At the same time, the DFN is more complex because its development based on two key factors, namely discontinuities network geometry and transmissivity of individual fractures. The latter is usually described quantitatively by cubic law, but the geometry of discontinuities network is varied. Ma et al. (2011) simplified coal was a collection of matchsticks, where each stick represented one coal matrix and the space between the sticks was representative of the discontinuities. Zhao et al. (2020) and Liu et al. (2018) regarded coal as 2D and 3D masonry structures, respectively. Based on micro-CT technology, Karimpouli et al. (2017) and Yu et al. (2019) calculated the distance and distribution of coal cleats, and developed a rectangular grid model that not only had geometrical statistics but also characterized the cleats.

As mentioned above, the linear elastic fracture theory and the 2D simplified DFN model are the two common assumptions to obtain the criterion for HFs crossing strata interfaces. However, these assumptions are not suitable for broken soft and low-permeability coal, because of its significant inelastic deformation, nonlinear fracture and complex 3D discontinuities network geometry. Although the elastic damage constitutive equations (Guo et al. 2017) and 3D DFN method based on computed tomography (CT) technology (Karimpouli et al. 2017; Yu et al. 2019) have been used to characterized the nonlinear fracture of rock and the cleat network of primary structure coal respectively, whether they can be applied to the broken soft and low-permeability coal needs further study. What's more, in addition to in-situ stress, mechanical strength of interface, scholars did not pay more attention to another factor that has a significant impact on the field-scale criterion of HFs crossing the coal–rock interface, that is, the distance between horizontal well and the interface (D_{op}, shown in Fig. 1c), which will greatly limit

the application of the existing laboratory-scale criterion (Jiang et al. 2019; Wang et al. 2018) in engineering practice.

In this article, Zhaozhuang mine in Qinshui basin is taken as the study area, where the coal is characterized by broken soft and low—permeability. To implement the indirect fracturing technology successfully, we focus on two key issues that determine the validity of the field-scale criterion, that is, the plasticity- nonlinear fracture -seepage (PF-S) coupled constitutive equations and 3D discontinuities network model for the coal. The adequacy of the two issues was verified by CT experiments, fracture mechanics tests and lab-scale HF experiments. On these bases, 115 numerical models with different in-situ stress, interface strength and D_{op} (Fig. 1c) were established, and the field-scale criterion of HFs crossing the coal–rock interface was obtained. Based on the "criterion", the indirect fracturing technology was successfully implemented in Zhaozhuang mine, and the CBM production was increased from 300 to 3000 m^3/day. The "field-scale criterion" is of great significance to popularize indirect fracturing coal technology and increase the CBM production in areas of broken soft and low-permeability coal.

2 The Study Area and its CBM Exploitation Status

In this article, Zhaozhuang coal mine was taken as the study area to investigate the key scientific problem of indirect fracturing coal technology, that is, the field-scale criterion of HFs crossing coal–rock interface.

2.1 Coalfield Geology of Study Area

Qinshui basin is the most important CBM production base in China (Zhang et al. 2017; Huang et al. 2019), and Zhaozhuang mine is located in the southeast of Qinshui basin. No. 3 coal is one of the main CBM reservoirs, with an average thickness of 4.95 m and the mining depth is about 450 m. There are no large faults and karst collapse columns in the north mine, which provide favorable conditions for No. 3 coal to become a high CBM bearing reservoir (the average CBM content is 12 m^3/t). Under the influence of regional tectonic stress, the primary structure of the coal is destroyed and become broken and soft, resulting in poor mechanical strength and significant inelastic deformation. In addition, the discontinuities are squeezed and closed under the action of in-situ stress. As a result, the coal permeability is usually less than 1 mD. The roof and floor of the coal bed are sandy mudstone, fine sandstone and mudstone respectively, and their parameters are shown in Fig. 2.

Comparing the coal parameters of Qinshui and San Juan basin, the mechanical strength and permeability of the former are much lower than those of the latter (Fig. 2). If the
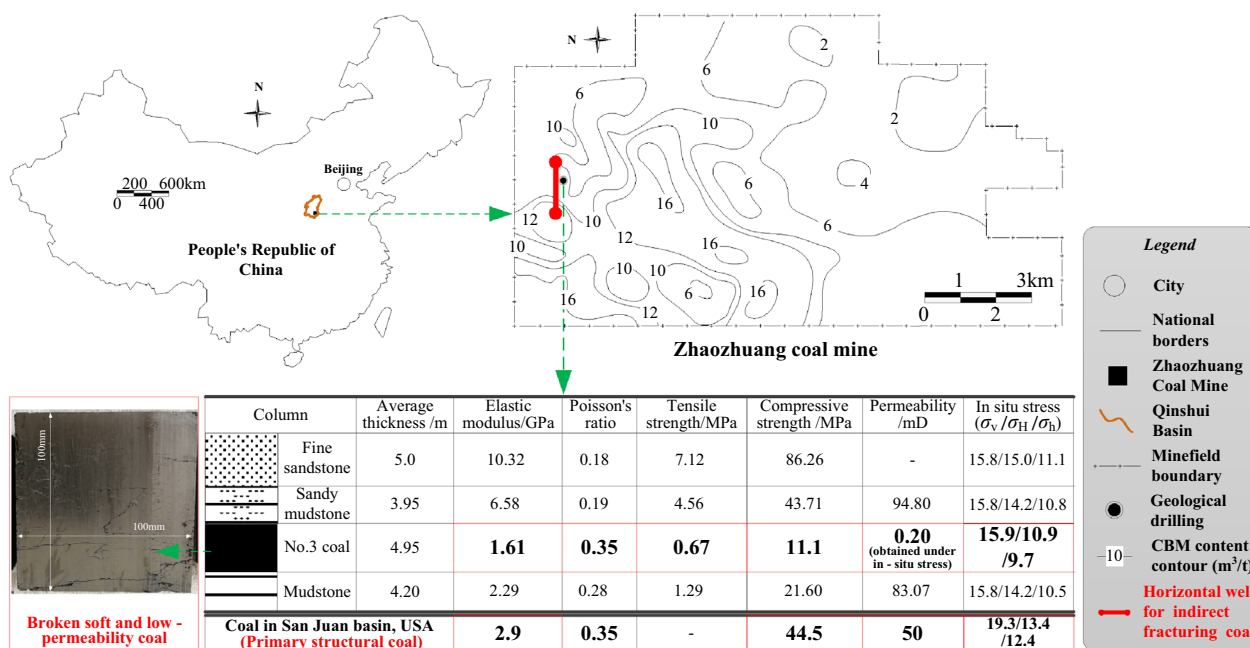
Fig. 2 The study area and its coalfield geological characteristics (Data related to the San Juan Basin are from Shi and Durucan 2004; Palmer et al. 2005)

direct fracturing coal technology widely used in San Juan basin is adopted in Qinshui basin, there will be three thorny difficulties:

(1) Horizontal well is easy to collapse;
(2) Under the preconditions of Zhaozhuang mine's existing ground equipment and restricted fracturing fluid types, the length of HFs in the coal is very short due to the inelastic deformation and nonlinear fracture of the coal;
(3) the order of resources development in Qinshui coalfield is exploiting CBM first and then excavating coal. This sequence will lead to a consequence that horizontal wells (including steel pipe and cement) will hinder coal mining if the direct fracturing coal technology is applied.

In terms of the CBM exploitation status Zhaozhuang mine, only 49 of the 250 wells that use direct fracturing coal technology can produce CBM. And the daily CBM production of 49 gas-producing wells is generally less than 300 m³, which declares the failure of direct fracturing coal technology.

2.2 Problems in Indirect Fracturing Coal Technology

The three difficulties mentioned in Sect. 2.1 can be effectively avoided when the indirect fracturing coal technology is applied (Fig. 1c). This technology is strongly supported by

the in-situ stress and excellent roof mechanical properties of the Zhaozhuang mine. As shown in Fig. 2, the vertical principal stress (σ_v) > the maximum horizontal principal stress (σ_H) > the minimum horizontal principal stress (σ_h) in the roof and coal. In addition, sandy mudstone is harder than coal, but softer than fine sandstone, which means that HFs are relatively easier to extend downward than upward (Afsar et al. 2011; Athavale and Miskimins 2008).

The bad news, however, is that the abundant discontinuities, inelastic deformation and nonlinear fracture characteristics of the coal may prevent HFs crossing the coal–rock interface. For brittle layered rocks, although most of hydraulic energy is converted into the fracture surface energy to promote the HFs propagation, the HFs are still not easy to cross the interface (Dehghan et al. 2015; Tan et al. 2017). Furthermore, the mixed fracture mode, significant inelastic deformation and nonlinear fracture characteristics of the coal will consume a lot of hydraulic energy, making it more difficult for HFs to cross the coal–rock interface. In addition, in-situ stress and interfacial shear strength, especially D_{op} (Fig. 1c), are the key factors affecting the successful crossing of HFs through the coal–rock interface in engineering practice, and the field-scale criterion under the influence of the three factors needs further research.

3 Methodology

Numerical simulation is a powerful tool to study the field-scale criterion of HFs crossing the coal–rock interface. To make the numerical simulation results more reliable, a novel 3D discontinuities network model based on CT experiment, and constitutive equations based on nonlinear mechanics and seepage theory suitable for the coal are established. The overview of the methodology is shown in Fig. 3.

3.1 3D Discontinuities Network Model Based on CT Experiment

The discontinuities are the important channel for the HFs propagation in the coal. The geometric parameters of coal discontinuities can be obtained by CT experiment, and the 3D discontinuities network model based on the results can be further applied to the HF problem in field-scale. The coal

Fig. 3 Overview of the methodology

specimens was processed into rectangular specimens along the parallel bedding direction, with length×width×height= 100 mm×100 mm×50 mm, and CT experiment was carried out after it was dry. The experiment was performed using nanovoxel-5000 3D computed tomography scanner from Sanying Precision Instruments Co. Ltd. Its voxel resolution is up to 500 nm, the maximum scanning voltage is 300 kV, and it can detect specimens with a length, width and height of less than 600 mm. The specific process, gray threshold determination method and discontinuities reconstruction method can be referred to the literature (He. 2018), and the main parameters of CT experiment were as follows: scanning voltage 270 kV, current 430 μA, exposure time 0.6 s, resolution 40 μm, and a set of data was generated for each 0.225° rotation of the specimen. The CT results of two coal samples are shown in Fig. 4a and b.

As shown in Fig. 4, the discontinuities of the broken soft and low-permeability coal in Zhaozhuang mine are usually does not penetrate the coal sample, but partially bonded and the remaining part is not bonded (the blue part in Fig. 4a). To facilitate the geometric parameters statistics of the defects and simplify the 3D model of discontinuities network, the non-bonded parts near the same plane are extended along the plane until they intersect with other planes (Yu et al. 2016). The resulting discontinuities network geometry of Zhaozhuang coal has the characteristics of 3D Voronoi polyhedron (Fig. 4c). In addition, the polyhedron is also suitable for the discontinuities network geometry of broken soft coal near Zhaozhuang mine, as shown in Fig. 5.

As shown in Figs. 4 and 5 3D discontinuities network model can well describe the spatial distribution of discontinuities of broken soft and low-permeability coal in or near the Zhaozhuang mine. The construction steps of voronoi polyhedron can be described as follows: (1) generating random points. In this article, the position of random points was determined by CT experiment, including the average spacing of random points in x, y and z direction (Fig. 4) are

(a) 3D reconstruction of discontinuities of specimen 1 **(b)** 3D reconstruction of discontinuities specimen 2 **(c)** 3D voronoi polyhedron network model of discontinuities
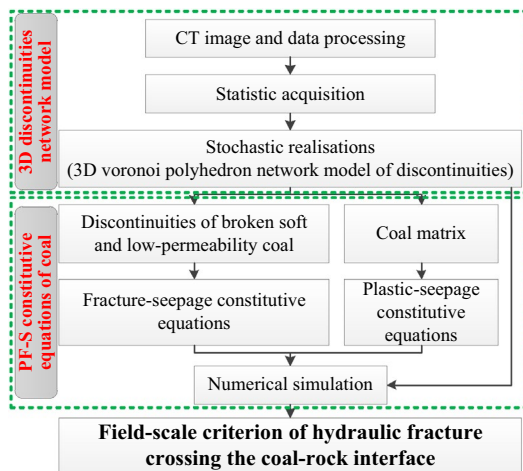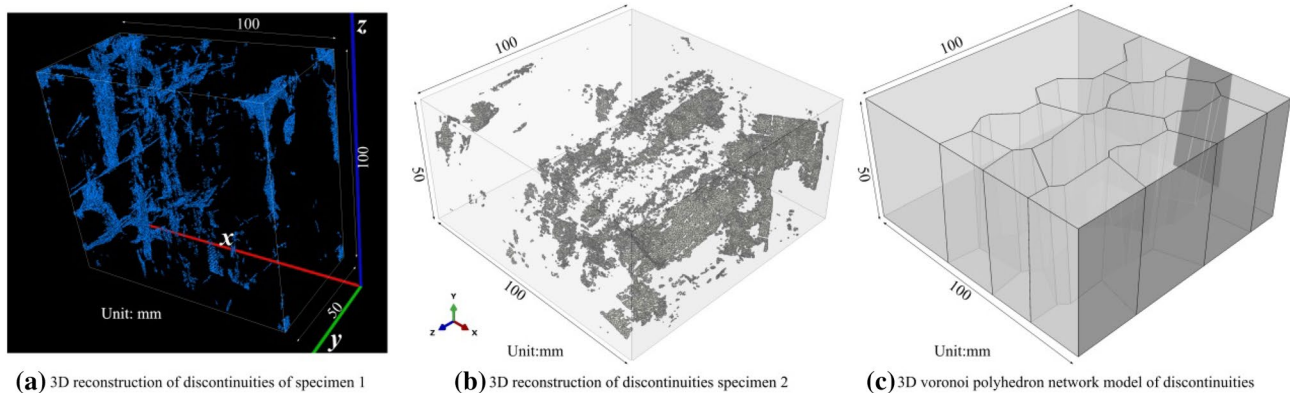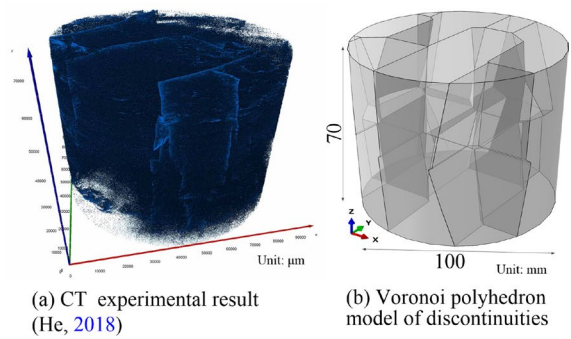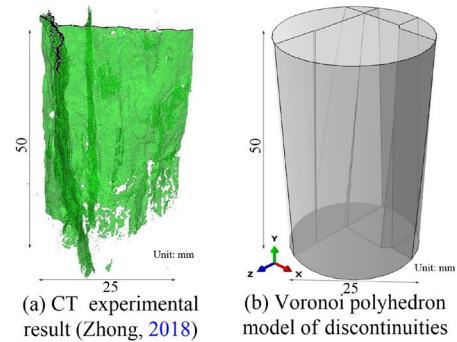
**Fig. 4** CT experimental results and simplified model of coal discontinuities in Zhaozhuang coal mine

Fig. 5 CT experimental results and 3D discontinuities network model of broken soft coal near the Zhaozhuang Mine

(a) CT experimental result (He, 2018)

(b) Voronoi polyhedron model of discontinuities

(I) WuYang Coal Mine

(a) CT experimental result (Zhong, 2018)

(b) Voronoi polyhedron model of discontinuities

(II) Tianan Coal Mine

(a) CT experimental result (Chu, 2018)

(b) Voronoi polyhedron model of discontinuities
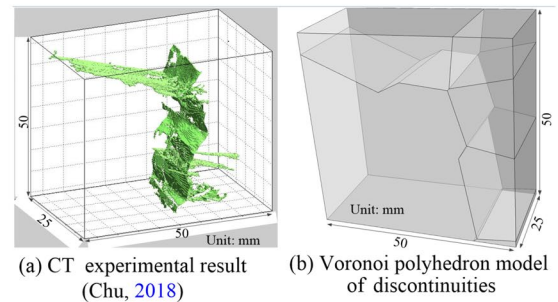
(III) Baishan Coal Mine

50 mm, 15 mm and 15 mm, and the fluctuation is 5 mm, 5 mm and 15 mm, respectively; (2) constructing Delaunay triangulation network by Delaunay algorithm (Shi 2019); (3) determining the circumscribed circle center of triangles; (4) connecting adjacent centers and generating voronoi polyhedron; and (5) deleting the faces of the voronoi polyhedron at intervals. According to the above steps, the positions of "random points" are the key factor to determine the geometric parameters of voronoi polyhedron. Therefore, the CT data (Fig. 4a and b) need to be statistically analyzed. The comparisons of discontinuities geometric parameters between CT experiment and 3D discontinuities network model are shown in Fig. 6.

It can be seen from Fig. 6 that the discontinuities spatial distribution (Fig. 4), and the statistical results of orientation (Fig. 6a), spacing (Fig. 6b), length (Fig. 6c) obtained from

CT data and 3D discontinuities model are generally consistent, which indicates that the 3D model can well describe the discontinuities network geometry of broken soft and low-permeability coal.

3.2 Constitutive Equations of Plasticity Fracture-Seepage (PF-S) for the Coal

The constitutive equations of broken soft and low-permeability coal are another core issue to determine the rationality of numerical simulation results. The coal is a typical pore—fracture medium (Izadi et al. 2011). Under this assumption, the plastic deformation and seepage characteristics of the coal matrix, as well as the nonlinear fracture and seepage characteristics of the discontinuities were studied respectively. Coupling constitutive equations of plasticity
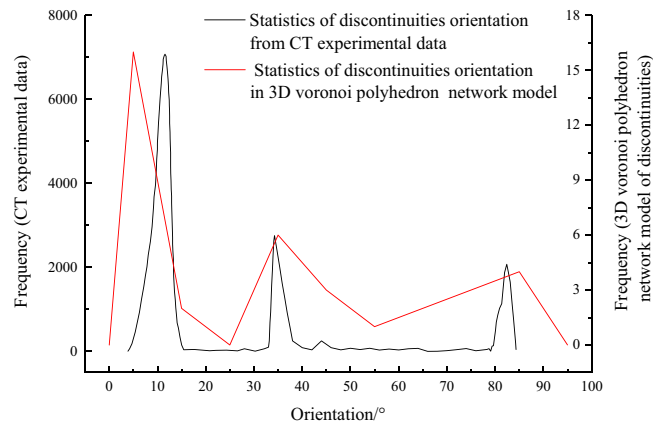
(a) Statistical results of discontinuities orientation (angle with *z* axis in Fig. 4)
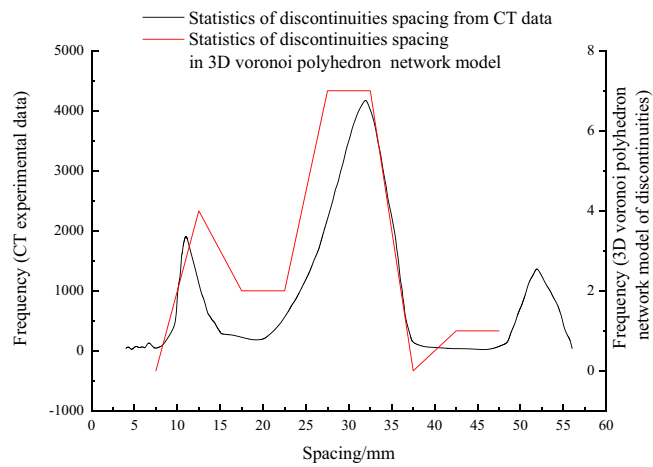
(b) Statistical results of discontinuities spacing
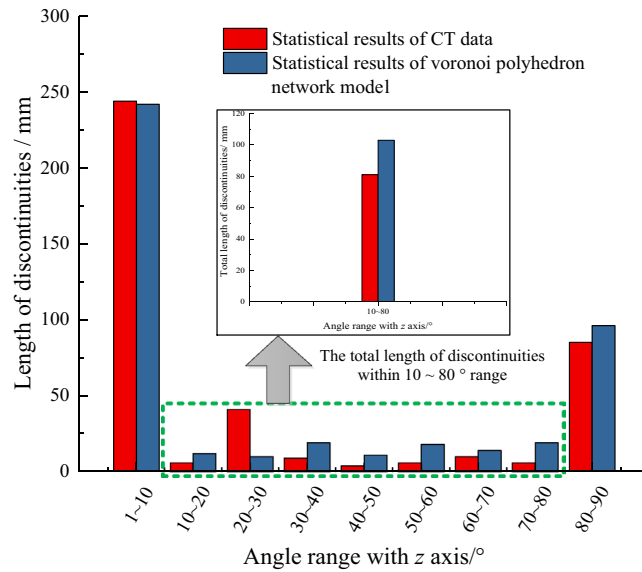
(c) Statistics of discontinuities length in different orientation

Fig. 6 Statistics of discontinuities geometric parameters in CT experiment and 3D discontinuities network model

fracture-seepage (PF-S equations) for coal were established as follows.

3.2.1 Hydro-mechanical Coupling of the Coal Matrix with Plastic Deformation Characteristics

To simulate the hydro-mechanical coupled behavior in coal matrix (i.e. solid elements in numerical model), three basic equations (Li et al. 2009) are adopted, including equilibrium equation (Eq. 1), geometric equation (Eq. 2) and continuity equation (Eq. 3).

$$\nabla \boldsymbol{\sigma}_s^t - \mathbf{F}_s = 0 \tag{1}$$

$$\boldsymbol{\varepsilon}_s = (\nabla \mathbf{u}_s + \mathbf{u}_s \nabla)/2 \tag{2}$$

$$\nabla q_{s,w} = -\frac{\partial \varepsilon_{s,v}}{\partial t} + \frac{\phi}{K_w} \frac{\partial p_{s,w}}{\partial t} \tag{3}$$

where $\boldsymbol{\sigma}_s^t$ is the total stress of solid element; $\mathbf{F}_s$ is the body force; $\boldsymbol{\varepsilon}_s$ is the strain vector, and $\varepsilon_{s,v}$ is the volumetric strain; $\mathbf{u}_s$ is the displacement vector; q_w is the seepage velocity; t is the time; and $p_{s,w}$ is the pore water pressure; ϕ is porosity; K_w is the bulk modulus of water.

The plastic damage-seepage constitutive model for coal matrix can be obtained by combining the Biot effective stress principle, damage and plastic mechanics theory as well as Darcy's law. The expression is shown in Eq. 4.

$$\boldsymbol{\sigma}_s^t = \boldsymbol{\sigma}_s^e + \alpha \mathbf{I} p_w = (1-d)\mathbf{D}_{0,s}(\boldsymbol{\varepsilon}_s - \boldsymbol{\varepsilon}_{s,p}) + \alpha \mathbf{I} p_w \tag{4}$$

where $\boldsymbol{\sigma}_s^e$ is effective stress vector; α is the Biot coefficient, and $\alpha = 1 - K_b/K_s$, K_s is the effective bulk modulus of the solid constituent, K_b is the drained bulk modulus of the porous medium; $\mathbf{D}_{0,s}$ is the undamaged elastic stiffness matrix of solid element; $\boldsymbol{\varepsilon}_{s,p}$ is the plastic strain vector; One of the unknown variables d is the damage value, which is the function of $\gamma_{p,c}^{eq}$, and:

$$d = (e^{-\gamma_{p,c}^{eq}/a} - 1)/(e^{-1/a} - 1) \tag{5}$$

where $\gamma_{p,c}^{eq}$ is a function of confining pressure σ_c, $\gamma_{p,c}^{eq} = \int d\gamma_p^{eq}/[b_1(\sigma_c/\sigma_{ucs}) + c_1], \gamma_p^{eq}$ is the equivalent shear plastic strain; σ_{ucs} is uniaxial compressive strength; a, b_1 and c_1 are constant, and can be obtained as follows: we can get the inelastic deformation and elastic modulus during each cycle by cyclic loading and unloading experiment, so that the curves of d-γ_p^{eq} and γ_p^{eq}-(σ_c/σ_{ucs}) can be obtained, and then fitting the two curves by linear functions, the three parameters can be deduced.

The other unknown variables $\boldsymbol{\varepsilon}_p$ in Eq. 4 can be solved based on the Mohr–Coulomb yield criterion (Eq. 6) and the non-associated flow rule (Eq. 7).

$$F = (\sigma_n^e tan\varphi + c) + d(p_w tan\varphi - c) - \tau^e = 0 \tag{6}$$

$$G = \sqrt{(\delta c tan\psi)^2 + (rq)^2} - ptan\psi \tag{7}$$

where, σ_n^e and τ^e are the normal and tangential effective stresses on the shear plane; φ, c are the internal friction angle, cohesive force, respectively; p^e and q^e are effective hydrostatic stress and the effective deviatoric stress; δ is eccentricity, which defines the rate at which the function approaches the asymptote, $\delta = 0.1$ (Fei and Zhang 2013); ψ is the dilation angle measured in the $p-q$ plane at high confining pressure; r controls the shape of the plastic potential surface in the deflection plane, and

$$r = \frac{r_c\left[4(1-e^2)cos^2\theta + (2e-1)^2\right]}{2(1-e^2)\cos\theta + (2e-1)\sqrt{4(1-e^2)cos^2\theta + 5e^2 - 4e}} \tag{8}$$

where r_c is the polar diameter under the polar coordinate system, its value can be obtained by the triaxial compression test; θ is the polar angle; e is the eccentricity of the partial plane, which controls the shape of the plastic potential surface in the range of $\theta = 0 - \pi/3$, and $e = 0.667$ (Fei and Zhang 2013).

The permeability coefficient of coal matrix will show significant difference between elastic and inelastic deformation, and the expression can be derived from Darcy's law and cubic law:

$$k = \begin{cases} k_{nd}\left\{ \left(1 + \varepsilon_{ve}\right)^3/\phi - (1-\phi)/\left[\phi\left(1 + \varepsilon_{ve}\right)^{1/3}\right] \right\}, \varepsilon_p = 0, \\ (1-d)k_{nd} + dk_d\left(1 + d\varepsilon_{vp,c}\right)^3, \varepsilon_p > 0 \end{cases} \tag{9}$$

where k_{nd} and k_d is the permeability coefficient of the non-damaged and damaged part; ε_{ve} is the elastic volume strain; $\varepsilon_{vp,c}$ is a function of σ_c, $\varepsilon_{vp,c} = \int d\varepsilon_{vp}/[b_2(\sigma_c/\sigma_{ucs}) + c_2], \varepsilon_{vp}$ is plastic volume strain, b_2 and c_2 are constant, and can be obtained using the same method as b_1 and c_1.

3.2.2 Hydro-Mechanical Coupling of the Discontinuities with Nonlinear Fracture Characteristics

Cohesive element fluid flow model can well reflect hydro-mechanical coupling behavior of discontinuities in rock (Ortiz and Pandolfi 2018). However, for the broken soft coal, the traction ($\boldsymbol{\sigma}_c$)—separation ($\boldsymbol{S}$) criterion under different fracture modes needs to be further improved to match the nonlinear fracture characteristics of the coal discontinuities.

The constitutive relationship before the peak load and the criterion for fracture initiation propagation can be determined by Eqs. 10–11 (Ortiz and Pandolfi 2018).

$$\boldsymbol{\sigma}_c = \mathbf{D}_{0,c} \boldsymbol{\varepsilon}_c \tag{10}$$

$$\max \left\{ \frac{\langle \sigma_{c,n} \rangle}{\sigma_{c,n}^0}, \frac{\sigma_{c,s}}{\sigma_{c,s}^0}, \frac{\sigma_{c,t}}{\sigma_{c,t}^0} \right\} = 1 \tag{11}$$

where $\sigma_{c,n}$, $\sigma_{c,s}$ and $\sigma_{c,t}$ (or $\sigma_{c,n}^0$, $\sigma_{c,s}^0$ and $\sigma_{c,t}^0$) are the (peak) traction in the normal and two tangential directions, respectively; the symbol $\langle \ \rangle$ is the Macaulay bracket; $\mathbf{D}_{0,c}$ is the elastic stiffness matrix, and E_{nn}, E_{ss} and E_{tt} are the elements on the diagonal of the matrix, representing the elastic modulus of normal, first tangent and second tangent respectively; $\boldsymbol{\varepsilon}_c$ is the strain vector, the relationship between $\boldsymbol{\varepsilon}_c$ and $\mathbf{S}$ is $\boldsymbol{\varepsilon}_c = \mathbf{S}/T_0$, T_0 is the constitutive thickness of cohesive element.

After the peak load, the strain softening constitutive model under different fracture modes can be deduced by the following method.

Considering mode I, II and III fractures, the Park-Paulino-Roesler (PPR) potential energy function of 2D problems (Park et al. 2008) can be extended to 3D problems. The expression of potential energy function $\Psi(S_n, S_S)$ is as follows:

where $S_S = \sqrt{S_s^2 + S_t^2}$, S_s and S_t are variables, which are the separation of the first and second tangential directions respectively; Γ_n, Γ_S are fracture energy constants, and

$$\Gamma_n = (-G_n)^{\langle G_n - G_S \rangle / (G_n - G_S)} \left(\frac{\beta}{m} \right)^m \quad \Gamma_S = (-G_S)^{\langle G_S - G_n \rangle / (G_S - G_n)} \left(\frac{\gamma}{n} \right)^n \tag{13}$$

where, G_n and G_S are normal and tangential fracture energies, and $G_S = G_s + G_t$, G_s and G_t are the first and second tangential fracture energies, respectively; β, γ are the shape index parameters of the traction—separation curve under pure tension and pure shear conditions respectively, which can be obtained by fitting the experimental data (Figs. 6, 7). The parameters m and n are related to β and γ, and the expressions are as follows:

$$\begin{cases} m = \beta(\beta - 1)\chi_n^2/(1 - \beta\chi_n^2) \\ n = \gamma(\gamma - 1)\chi_S^2/(1 - \gamma\chi_S^2) \end{cases} \tag{14}$$

where parameters $\chi_n = s_{n,p}/s_n$, $\chi_S = s_{S,p}/s_S$, they determine the amount of separation corresponding to the peak load; $s_{n,p}$ and $s_{S,p}$ are the displacements corresponding to peak normal load and peak tangential load, respectively.

$$\Psi(S_n, S_S) = \left[\Gamma_n \left(1 - \frac{S_n}{s_n} \right)^\beta \left(\frac{m}{\beta} + \frac{S_n}{s_n} \right)^m + \langle G_n - G_S \rangle \right] \times \left[\Gamma_S \left(1 - \frac{|S_S|}{s_S} \right)^\gamma \left(\frac{n}{\gamma} + \frac{|S_S|}{s_S} \right)^n + \langle G_S - G_n \rangle \right] + min(G_n, G_S) \tag{12}$$

By calculating the first derivative of $\Psi(S_n, S_S)$, the constitutive equations of different fracture modes can be obtained, as shown in Eqs. (15–17).

$$\sigma_{c,n} = \frac{\Gamma_n}{s_n} \left\{ m \left(1 - \frac{S_n}{s_n} \right)^\beta \left(\frac{m}{\beta} + \frac{S_n}{s_n} \right)^{m-1} - \beta \left(1 - \frac{S_n}{s_n} \right)^{\beta-1} \left(\frac{m}{\beta} + \frac{S_n}{s_n} \right)^m \right\} \tag{15}$$
$$\times \left[\Gamma_S \left(1 - \frac{\sqrt{S_s^2 + S_t^2}}{\sqrt{s_s^2 + s_t^2}} \right)^\gamma \left(\frac{n}{\gamma} + \frac{\sqrt{S_s^2 + S_t^2}}{\sqrt{s_s^2 + s_t^2}} \right)^n + \langle G_s + G_t - G_n \rangle \right]$$

$$\sigma_{c,s} = \frac{\Gamma_S}{\sqrt{s_s^2 + s_t^2}} \left[\Gamma_n \left(1 - \frac{S_n}{s_n} \right)^\beta \left(\frac{m}{\beta} + \frac{S_n}{s_n} \right)^m + \langle G_n - G_s - G_t \rangle \right]$$
$$\times \left\{ n \left(1 - \frac{\sqrt{S_s^2 + S_t^2}}{\sqrt{s_s^2 + s_t^2}} \right)^\gamma \left(\frac{n}{\gamma} + \frac{\sqrt{S_s^2 + S_t^2}}{\sqrt{s_s^2 + s_t^2}} \right)^{n-1} \frac{S_s}{\sqrt{S_s^2 + S_t^2}} - \gamma \left(1 - \frac{\sqrt{S_s^2 + S_t^2}}{\sqrt{s_s^2 + s_t^2}} \right)^{\gamma-1} \left(\frac{n}{\gamma} + \frac{\sqrt{S_s^2 + S_t^2}}{\sqrt{s_s^2 + s_t^2}} \right)^n \frac{S_s}{\sqrt{S_s^2 + S_t^2}} \right\} \tag{16}$$

Fig. 7 Numerical calculation process of PF-S constitutive model
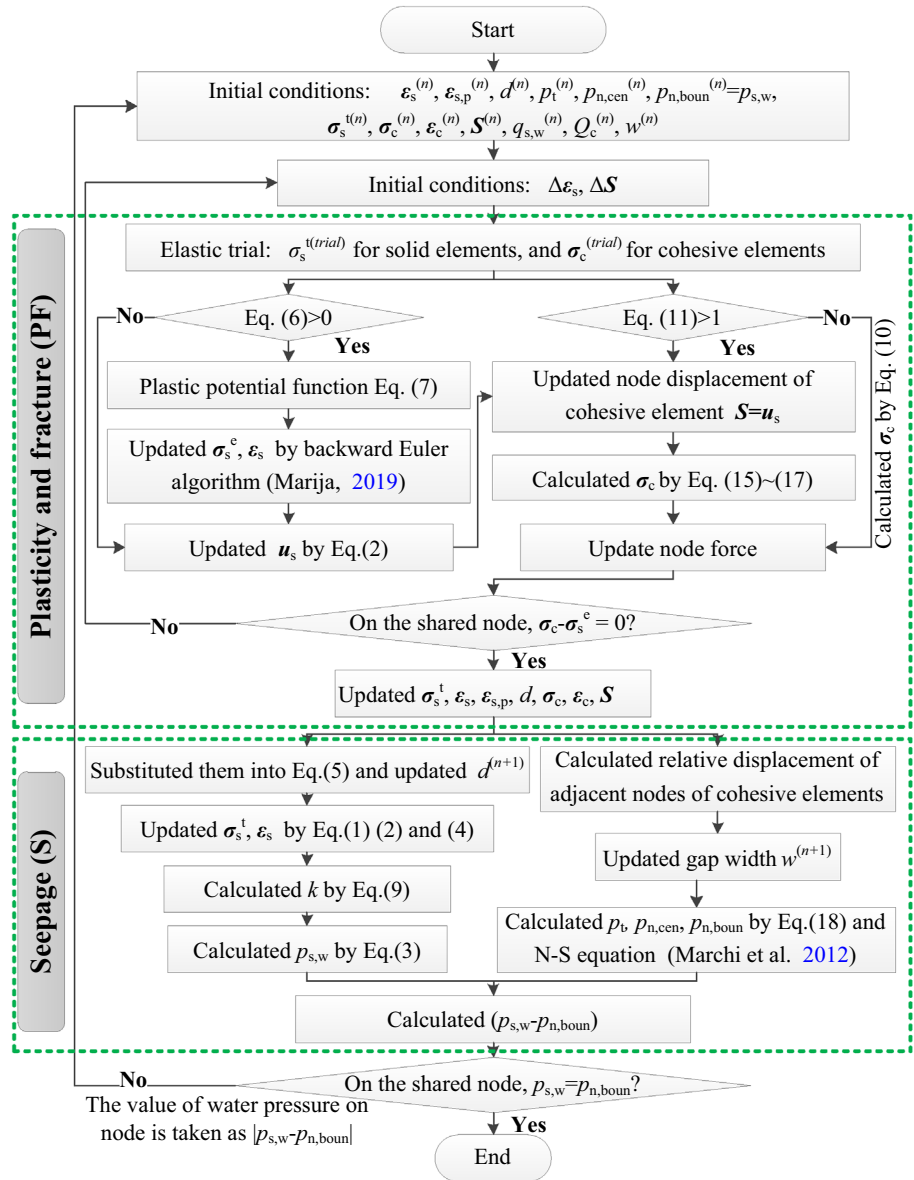
$$
\sigma_{c,t} = \frac{\Gamma_t}{\sqrt{s_s^2 + s_t^2}} \left[\Gamma_n \left(1 - \frac{S_n}{s_n} \right)^\beta \left(\frac{m}{\beta} + \frac{S_n}{s_n} \right)^m + \langle G_n - G_s - G_t \rangle \right]
$$

$$
\times \left\{ n \left(1 - \frac{\sqrt{S_s^2 + S_t^2}}{\sqrt{s_s^2 + s_t^2}} \right)^\gamma \left(\frac{n}{\gamma} + \frac{\sqrt{S_s^2 + S_t^2}}{\sqrt{s_s^2 + s_t^2}} \right)^{n-1} \frac{S_t}{\sqrt{S_s^2 + S_t^2}} - \gamma \left(1 - \frac{\sqrt{S_s^2 + S_t^2}}{\sqrt{s_s^2 + s_t^2}} \right)^{\gamma-1} \left(\frac{n}{\gamma} + \frac{\sqrt{S_s^2 + S_t^2}}{\sqrt{s_s^2 + s_t^2}} \right)^n \frac{S_t}{\sqrt{S_s^2 + S_t^2}} \right\}
$$

(17)

In particular, if $S_s = S_t = 0$, $S_n = S_t = 0$, $S_n = S_s = 0$ in Eqs. (15–17), the stress expressions for mode I, II and III fracture modes can be obtained.

Elastic energy and inelastic energy can be obtained by integrating the traction–separation curves (Fig. 8Id, IId and IIId) before and after the peak load, respectively.

In addition to the fracture mechanics equations of discontinuities, the incompressible water in fractures should

Fig. 8 Comparison of fracture mechanics experimental and numerical simulation results

(a) Size of specimen or numerical model with mode I fracture

(b) Specimen and fracture pattern of laboratory test (Yang, 2019)

(c) Numerical calculation model and fracture pattern

(d) Comparison of traction - separation curves obtained by two methods
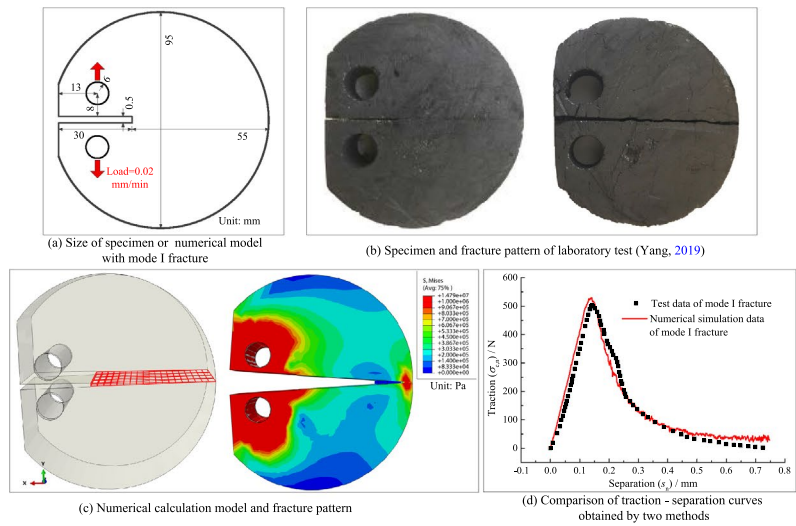
(I) Results of mode I fracture

(a) Size of specimen or numerical model with mode II fracture (The left side is the top view of the specimen, and the right side is the B-B section)

(b) Specimen and fracture pattern of laboratory test (Yang, 2019)

(c) Numerical calculation model and fracture pattern

(d) Comparison of traction - separation curves obtained by two methods
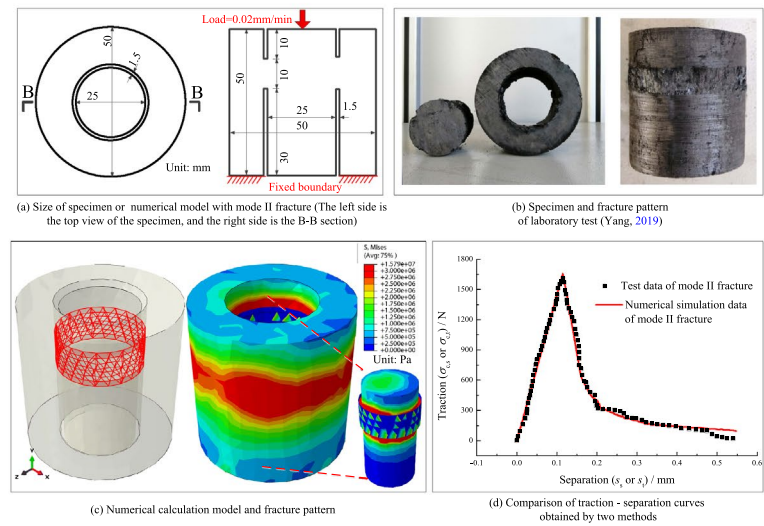
(II) Results of mode II fracture

(a) Size of specimen or numerical model with mixed-mode fracture

(b) Specimen and fracture pattern of laboratory test (Yang, 2019)

(c) Numerical calculation model and fracture pattern

(d) Comparison of load - CMOD curves obtained by two methods
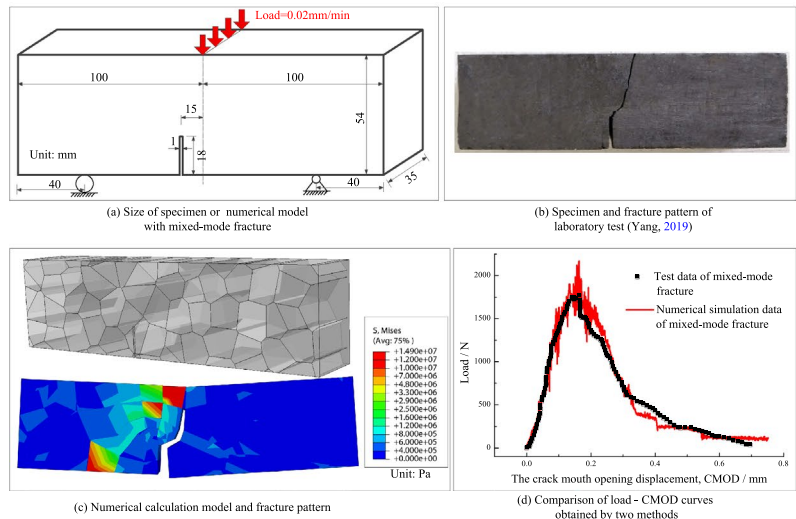
(III) Results of mixed-mode fracture

also satisfy the continuity equation. Based on the cubic law and considering the water leak-off effect, the expression is as follows:

$$\frac{\partial w}{\partial t} + 2k(p_{n,cen} - p_{n,boun}) = \frac{1}{12\mu}\nabla(w^3\nabla p_t) + Q_c\delta(x,y) \quad (18)$$

where Q_c is the total flow at the gap entrance; w is the gap width; μ is the dynamic viscosity of water; ∇p_t is the pressure gradient of tangential flow; ρ_w is the water density; g is acceleration of gravity; $p_{n,cen}$ and $p_{n,boun}$ are the water pressure in the middle gap and on the gap boundary; k is the leak-off coefficient or the permeability coefficient of coal matrix (Eq. 9).

Based on above equations, the PF-S constitutive equations are established, and the numerical calculation process is shown in Fig. 7.

4 Adequacy of PF-S equations

The adequacy of 3D discontinuities network model of the broken soft and low—permeability coal has been verified by CT experiments (Sect. 3.1). In the following, fracture mechanics tests and hydraulic fracturing experiments were used to verify the adequacy of the PF-S constitutive equations.

4.1 Results of Mode I, II and Mode Mixed Fracture of Coal

The field-scale numerical simulation results of HFs can be directly affected by the nonlinear fracture mechanical properties of the coal. The applicability of Eqs. (10–17) and the fracture mechanical parameters (Table 1) of the coal can be obtained by three-point bending and punch-through shear tests (Fig. 8Ib–IIIb, Yang 2019). It should be noted that the parameters of the cohesive elements in Table 1 have been converted to that of cohesive elements per unit area. According to the boundary conditions, loading modes and the specimens size used in the tests, the numerical calculation models were established. As shown in Fig. 8Ic–IIIc, the red highlighted part in the calculation models are the cohesive elements, and the Eqs. (10–18) were used to simulate the nonlinear fracture properties of these potential fracture surface; the other parts are solid elements, and the Eqs. (1–9) were used to simulate the plastic mechanical properties of coal matrix. The mechanical parameters of coal matrix and discontinuities are shown in Table 1. The results of experiment and numerical simulation based on the PF-S constitutive equations are shown in Fig. 8.

As shown in Fig. 8, the numerical simulation results of mode I and mode II fracture are highly consistent with the

experimental results since the fracture mechanical parameters of materials are obtained through fracture experiments. Although traction–separation expressions (Eqs. 15–17) of mixed fracture mode (Fig. 8) are derived theoretically, if the numerical simulation and experiment have the same fractures pattern, then the load-CMOD curve obtained by numerical simulation is close to the experimental results, which indicates the adequacy of the nonlinear fracture constitutive equations for the discontinuities of broken soft coal in the PF-S model. Comparing the fracture energy of the mode mixed (Fig. 8IIId) and the mode I (Fig. 8Id), that is, the area under the curve, the former is 2.62 times that of the latter, which means that the mixed mode fracture mode consumes more energy.

It should be emphasized that the simulation results shown in Fig. 8 is based on the hypothesis that a fracture can only develop by activating a pre-existing discontinuity. This hypothesis is based on two experimental results: (1) there are abundant discontinuities in the broken soft coal (Fig. 4), which is main mechanical weakness of the coal; (2) in the broken soft coal, HFs mainly propagate along the pre-existing fractures. The former has been described in Sect. 3.1, and the latter is illustrated by hydraulic fracturing experiments (Sect. 4.2).

4.2 Laboratory-Scale HF Results

On the basis of the fracture mechanics experiments in Sect. 4.1, laboratory-scale HF experiments can further verify the adequacy of the PF-S constitutive equations. The test samples, equipment, scheme and results are described below.

Coal-rock composite specimens (Fig. 9b) were the research object of lab-scale HF experiments. Between them, coal was taken from Zhaozhuang mine (Fig. 2), the roof was replaced by cement with the same mechanical properties to control the fluctuation of experimental data caused by the strong discreteness of roof mechanical parameters. And the two were connected by contact (without lubricant), oil grease and vaseline. The specimens were prepared according to the following steps: (1) The coal and cement was processed into a cuboids with the with length × width × height = 100 mm × 100 mm × 50 mm; (2) A hole with diameter × depth = 6 mm × 25 mm was drilled in cement specimens (Fig. 9c); (3) A steel pipe with an outer/inner diameter of 4 mm/3 mm and a length of 150 mm was placed in the borehole then sealed with high-strength resin, the fracturing section of 5 mm was left at the borehole bottom; (4) The coal–rock composite specimens were formed by connecting coal and cement.

Triaxial compression hydraulic fracturing seepage machine named TCHFSM-I (Fig. 9a and d) was employed to carry out the HF experiments. The maximum load of the machine in five directions is 3000 kN, the loading accuracy

Table 1 Numerical calculation parameters

	ϕ/%	E_s/GPa	μ	φ/°	c/MPa	ψ/°	a	b_1	c_1	c_2	b_2	δ	e	$k_0(k_1)$/10^{-10} ms^{-1}	k_2/10^{-7} ms^{-1}
Coal matrix	8.9	1.61	0.35	35	2.6	20	0.01	4.12	4.83	0.37	0.21	0.1	0.67	1.2	3.1
Roof	7.9	6.58	0.19	27	7.1	28	0.01	7.82	6.06	0.74	0.33	0.1	0.67	0.43	0.22

	E_n/GPa	E_{tt}/GPa	E_{ss}/GPa	$\sigma^0_{c,n}$/MPa	$\sigma^0_{c,s}$/MPa	$\sigma^0_{c,t}$/MPa	s_n/10^{-4} m	s_S/10^{-4} m	$s_{n,p}$/10^{-4} m	$s_{S,p}$/10^{-4} m	G_n/(N/m)	G_S/(N/m)	T_0
Discontinuity (coal)	0.98	1.83	1.83	0.67	1.06	1.06	3.2	5.9	0.61	1.78	57.74	343.05	1

	β	γ	χ_n	χ_S	m	n	Γ_n	Γ_S	l/m^3/(s·MPa)
Discontinuity (coal)	3.56	3.36	0.19	0.29	0.3	0.94	2.72	−1132.5	1.2×10^{-10}

is 0.01 kN/s, and the square-cavity can accommodate cube specimen with edge length of 100–400 mm. The maximum flow rate of constant flow pump is 200 ml/min, injection pressure in fracturing section can be monitored during the experimental process.

The procedure for the experiments follows Kim and Abass's advice (1991). First, σ_v, σ_H, σ_h increased from zero to the target values of test scheme σ'_h. Second, kept σ_h constant and increased σ_v, σ_H to σ'_H. Third, kept σ_h, σ_H constant, and increased the σ_v to σ'_v. The HF experiments were carried out after the specimens maintained in this stress state for 30 min. The fracturing fluid was water and the flow rate was controlled at 20 ml/min. Other experimental parameters are shown in Table 2. The frictional mechanics properties of three types of interfaces under different normal stress are shown in Fig. 10 (Jiang et al. 2019).

For numerical simulation, the size of the specimen is shown in Fig. 11. The distribution of coal discontinuities is shown in Fig. 4c, while the discontinuities in cement were arranged in its middle part and along with the direction of σ_H. Considering the small width of discontinuity (average value was 0.8 μm), and the discontinuities would be closed under stress, 0-thickness cohesive elements were embedded at the discontinuities position of the coal and cement. The rest parts are coal and cement matrix, which were represented by solid elements.

The constitutive equations and mechanical parameters of coal have been described in Sect. 4.1. For the elastic brittle cement, Eqs. (10, 11 and 18) were used for its cohesive elements, and Eqs. (1–4 and 9) (where $d=0$) were used for its solid elements. The elastic modulus and tensile strength of cement were 3 times of coal, and the fracture displacement was 1/2 of coal. The mechanical behavior of coal–rock interface was described by PF-S constitutive equations, and the shear strength of the three types of interfaces can be calculated according to Fig. 10, while the shear modulus under different normal stresses (σ_n) can be obtained by direct shear test, and the expressions are $E_{ss}=E_{tt}=0.032\sigma_n-0.018$ (interface without lubricant, unit: GPa), $E_{ss}=E_{tt}=0.00154\sigma_n-0.00884$ (oil grease interface, unit: GPa), $E_{ss}=E_{tt}=0.0011\sigma_n-0.00172$ (vaseline interface, unit: GPa), E_{nn} is 1/3 of that of coal. At the same time, $s_n=s_{n,p}$ and $s_S=s_{S,p}$ for the interface. The material parameters for coal are shown in Table 1. The boundary conditions of the numerical calculation model (Fig. 11) are as follows: the normal displacements of six surfaces of the numerical model were constrained respectively. The excess pore water pressure was set as 0, the pore ratio of cement and coal was set as 0.2 and 0.01 respectively, and the saturation was set as 1. The injection flow rate and initial stress conditions were the same as the HF experiments. The results of HF experiments (Jiang et al. 2019) and numerical simulation under
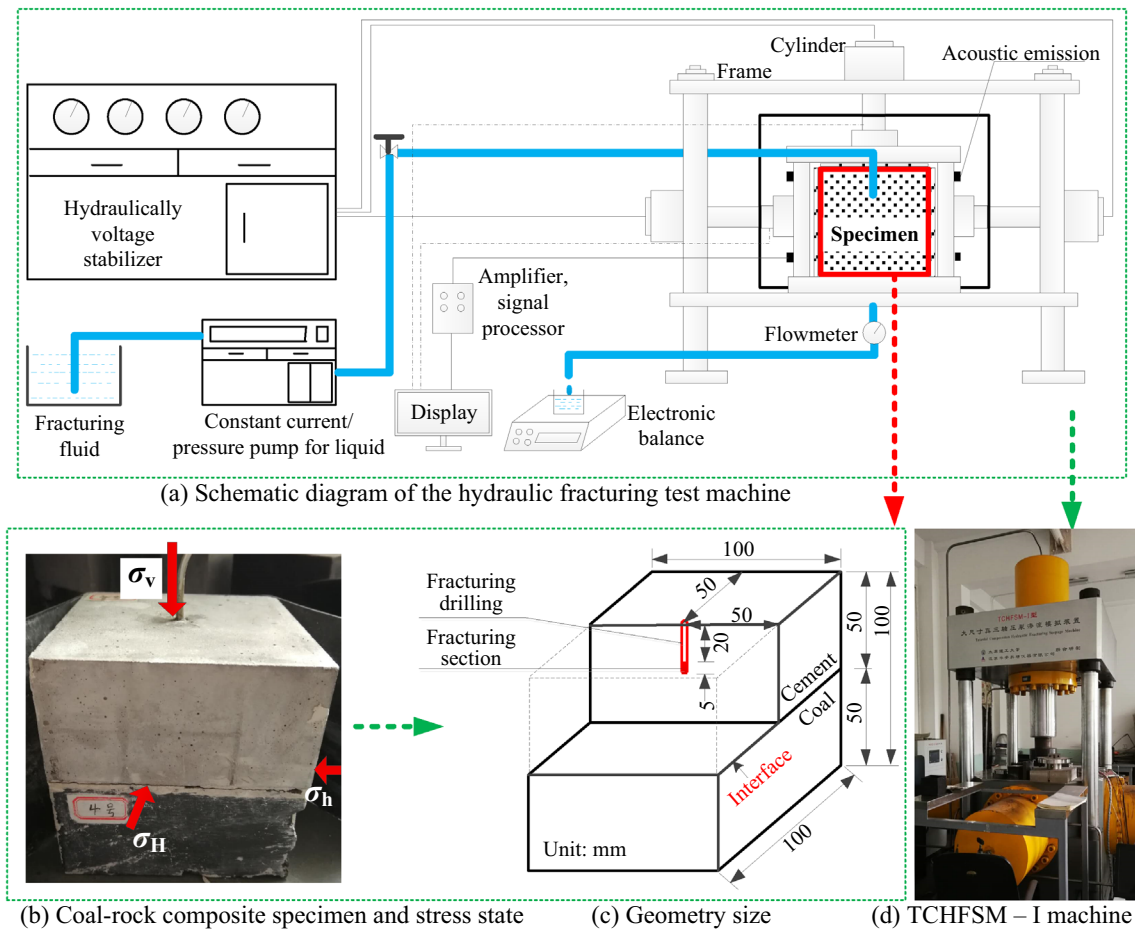
(a) Schematic diagram of the hydraulic fracturing test machine

(b) Coal-rock composite specimen and stress state (c) Geometry size (d) TCHFSM – I machine

Fig. 9 Test samples and triaxial compression hydraulic fracturing seepage machine

different stress states and interface properties are shown in Fig. 12.

The distribution of coal discontinuities in 28 # and 5 # specimens (Fig. 12) used in HF experiments are shown in Fig. 4a and b, and there are obvious discontinuities in the middle of specimens. Although the HFs in 28 # and 5 # cement deviate from the middle, the main HFs in coal still propagate along the pre-existing discontinuities instead of the intact interval. Therefore, an important hypothesis was put forward: in the broken soft and low-permeability coal, HFs mainly propagate along the pre-existing discontinuities, as Detournay (2016) discussed in the literature.

Comparing the results of experiment and numerical simulation, the stress difference threshold $\Delta\sigma^{thre}$ of HFs crossing coal–rock interface is consistent, which reflects the adequacy of PF-S constitutive equations. As shown in Fig. 12I, under the condition of interface without lubricant, HFs are only observed in the cement of 24# specimen (σ_v, σ_H, σ_h = 8, 5, 3 MPa); when the σ_v is increased to 9 MPa (the stress difference $\Delta\sigma = \sigma_v - \sigma_h = 6$ MPa), the HFs appear not only in the cement of 28#, but also in the coal, which indicates the

$\Delta\sigma^{thre}$ of HF crossing coal–rock interface under the condition of interface without lubricant is 6 MPa. When the interface is oil grease (Fig. 12II) and vaseline interface (Fig. 12III), the $\Delta\sigma^{thre}$ are 11 MPa and 15 MPa, respectively. In other words, the stress threshold increases with the decrease of the interface shear strength.

The curves of water pressure–time at water injection point obtained by experiment and numerical simulation are also similar. Take Fig. 12Id as an example, the curves can be divided into three stages: (1) the increasing stage (a–b stage). With the increase of water volume at the injection point, the water pressure increases gradually; (2) the descending stage (b–c stage). When the water pressure reaches the critical crack initiation condition of cement (point b), water pressure decreases rapidly, and then the HF reaches the coal rock interface at point c; (c) the fluctuation stage (c–d–e stage). The fundamental reason of water pressure fluctuation is that the mixed fracture mode is more hydraulic energy consuming. Specifically, when the fracture mode I appears, HFs are easier to expand, resulting in the decrease of water pressure; while HFs are difficult to expand when the discontinuities

Table 2 Hydraulic fracturing test scheme

Specimen	Interface type	Stress/MPa			Specimen	Interface type	Stress/MPa		
		σ_v	σ_H	σ_h			σ_v	σ_H	σ_h
1#	Lubricating oil	11	5	3	26#	Without lubricant	9	5	3
2#		11	5	3	27#		9	5	3
3#		11	5	3	28#		9	5	3
4#		8	5	3	34#	Vaseline	13	5	3
5#		8	5	3	35#		14	5	3
6#		7	5	3	36#		14	5	3
22#	Without lubricant	7	5	3	37#		15	5	3
23#		7	5	3	38#		15	5	3
24#		8	5	3	39#		15	5	3
25#		8	5	3					

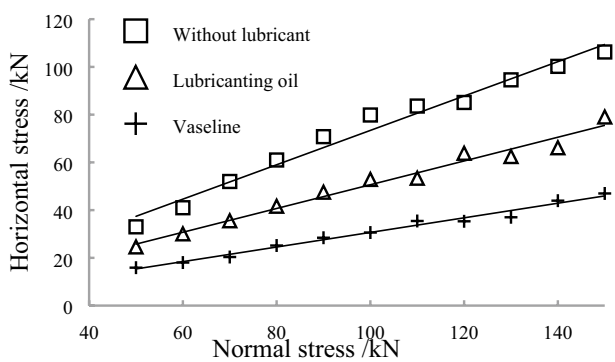**Fig. 10** The relationship between the maximum shear stress and normal stress at different interfaces (Jiang et al. 2019)

Fig. 11 Lab-scale numerical calculation model of HF

guide HFs to become a mixed fracture mode, resulting in the accumulation of hydraulic energy, and the water pressure will increase until new fractures occur. The water pressure in d-e stage is less than that in point d. For the case that the coal–rock interface is not crossed under the same stress and interface conditions (Fig. 12Ic), the water pressure at point d is not the peak point of the whole c–d–e stage, and the fluctuation times is less than the case of crossing the coal–rock interface. It is worth noting that the time corresponding to the peak point of water pressure (i.e. point b in the water pressure–time curve in Fig. 12) obtained by experiments and numerical simulation are not consistent, because the former used the non-saturated specimens, while the latter used the saturated hypothesis to simplify the calculation.

5 Field-Scale Criterion of Hydraulic Fracture Crossing Coal–Rock Interface

Although we have demonstrated that the coal–rock interface can hinder the HFs propagation in the lab-scale simulation and HF experiments, a field-scale study is essential because the D_{op} (Fig. 1c) vary greatly on different scales. Considering that the fracturing fluid is limited to water by engineers of Zhaozhuang mine, and the injection rate is restricted by the power of surface equipment, this section only studies the field-scale criterion of HFs crossing the coal–rock interface under the influence of three factors, including in-situ stress, the D_{op}, and the mechanical properties of coal–rock interface.

5.1 Field-Scale Numerical Calculation Model

There are few geological structures (such as faults and karst collapsed columns) in the north of Zhaozhuang mine, but there are several secondary folds. This article believes that the small geological structure has little influence on the
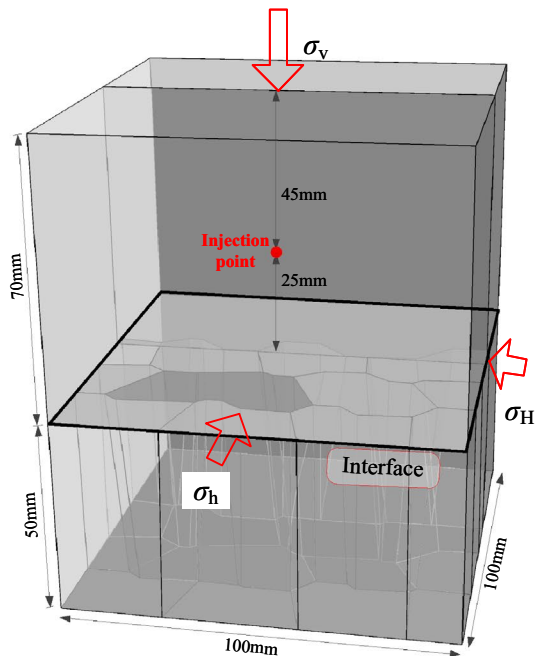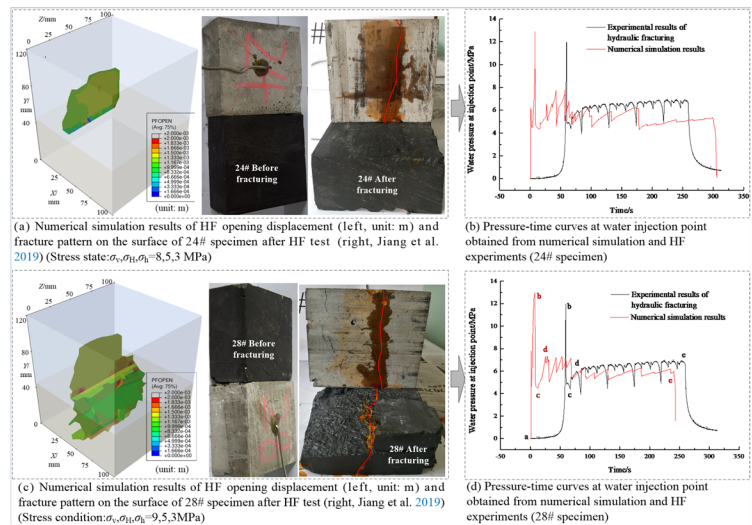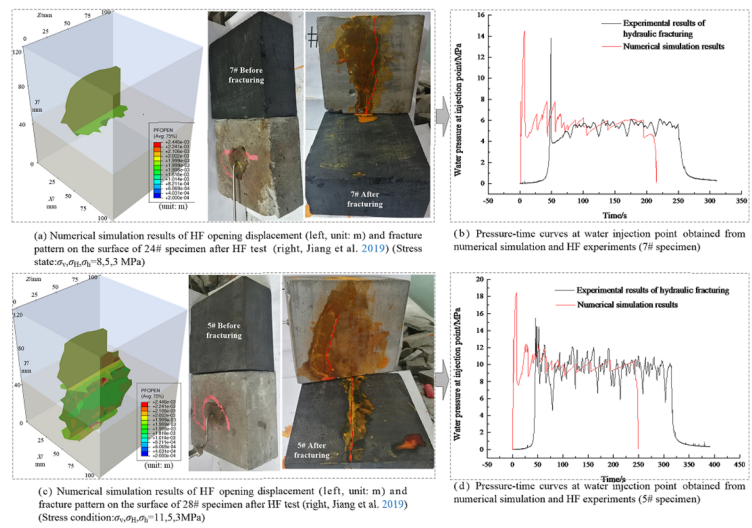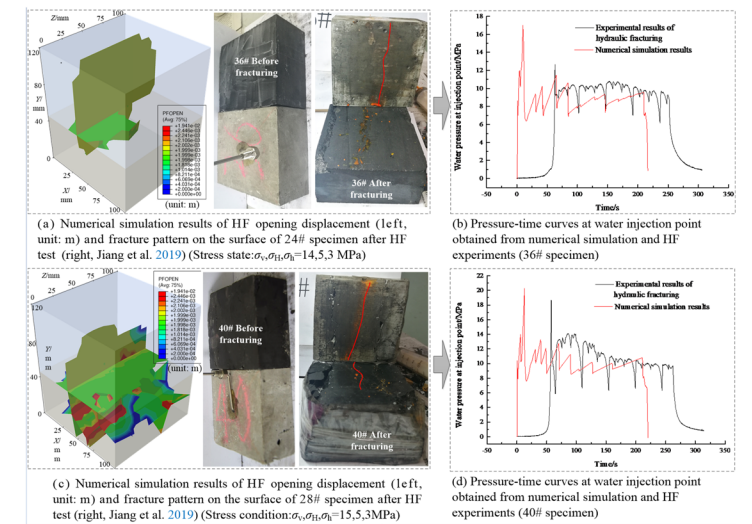
Fig. 12 The results comparison between numerical simulation and experiments of hydraulic fracturing

(a) Numerical simulation results of HF opening displacement (left, unit: m) and fracture pattern on the surface of 24# specimen after HF test (right, Jiang et al. 2019) (Stress state:σ_v,σ_H,σ_h=8,5,3 MPa)

(b) Pressure-time curves at water injection point obtained from numerical simulation and HF experiments (24# specimen)

(c) Numerical simulation results of HF opening displacement (left, unit: m) and fracture pattern on the surface of 28# specimen after HF test (right, Jiang et al. 2019) (Stress condition:σ_v,σ_H,σ_h=9,5,3MPa)

(d) Pressure-time curves at water injection point obtained from numerical simulation and HF experiments (28# specimen)

(I) Interface without lubricant

(a) Numerical simulation results of HF opening displacement (left, unit: m) and fracture pattern on the surface of 24# specimen after HF test (right, Jiang et al. 2019) (Stress state:σ_v,σ_H,σ_h=8,5,3 MPa)

(b) Pressure-time curves at water injection point obtained from numerical simulation and HF experiments (7# specimen)

(c) Numerical simulation results of HF opening displacement (left, unit: m) and fracture pattern on the surface of 28# specimen after HF test (right, Jiang et al. 2019) (Stress condition:σ_v,σ_H,σ_h=11,5,3MPa)

(d) Pressure-time curves at water injection point obtained from numerical simulation and HF experiments (5# specimen)

(II) Oil grease interface

(a) Numerical simulation results of HF opening displacement (left, unit: m) and fracture pattern on the surface of 24# specimen after HF test (right, Jiang et al. 2019) (Stress state:σ_v,σ_H,σ_h=14,5,3 MPa)

(b) Pressure-time curves at water injection point obtained from numerical simulation and HF experiments (36# specimen)

(c) Numerical simulation results of HF opening displacement (left, unit: m) and fracture pattern on the surface of 28# specimen after HF test (right, Jiang et al. 2019) (Stress condition:σ_v,σ_H,σ_h=15,5,3MPa)

(d) Pressure-time curves at water injection point obtained from numerical simulation and HF experiments (40# specimen)

(III) Vaseline interface

geometric distribution of coal discontinuities, thus the 3D discontinuities network model (Sect. 3.1) is suitable for the coal bed in field-scale. At the same time, it is necessary to fully consider the impact of coal–rock interface bonding and in-situ stress caused by folds. On this basis, a field-scale numerical model was established (Fig. 13Ia). The model contains fine sandstone, sandy mudstone, coal and mudstone successively from top to bottom. The directions of σ_v, σ_H, σ_h were applied along the y, z and x directions respectively, but the magnitude of σ_v, σ_H, σ_h in different strata were different, as shown in Fig. 2. The injection point was arranged at the center of x–z plane and 0.5 m, 1 m, 1.5 m, 2 m, 2.5 m away from coal–rock interface. An initial fracture zone of 0.5 m in length and 0.01 m in diameter was arranged below the injection point to match the geometric parameters of perforation in engineering practice. Water was injected with an injection rate of 8 m³/min and the injection duration of 100 min. The materials parameters are shown in Table 2 and Sect. 4.2. And boundary conditions of the numerical model are consistent with those described in Fig. 12. However, compared with the lab-scale numerical model (Fig. 11), we have to make a certain compromise with the field-scale numerical model because the highly nonlinear constitutive equations make the calculation cost quite high. Thus, specific measures are taken: including (1) the distance between coal discontinuities is expanded by 10 times, that is, 20 cm, which is consistent with the length of natural fracture of coal during core drilling; (2) the numerical calculation model is controlled at 10 m (x) × 14 m (y) × 20 m (z).

5.2 Field-Scale Criterion of Hydraulic Fracture Crossing Coal-Rock Interface
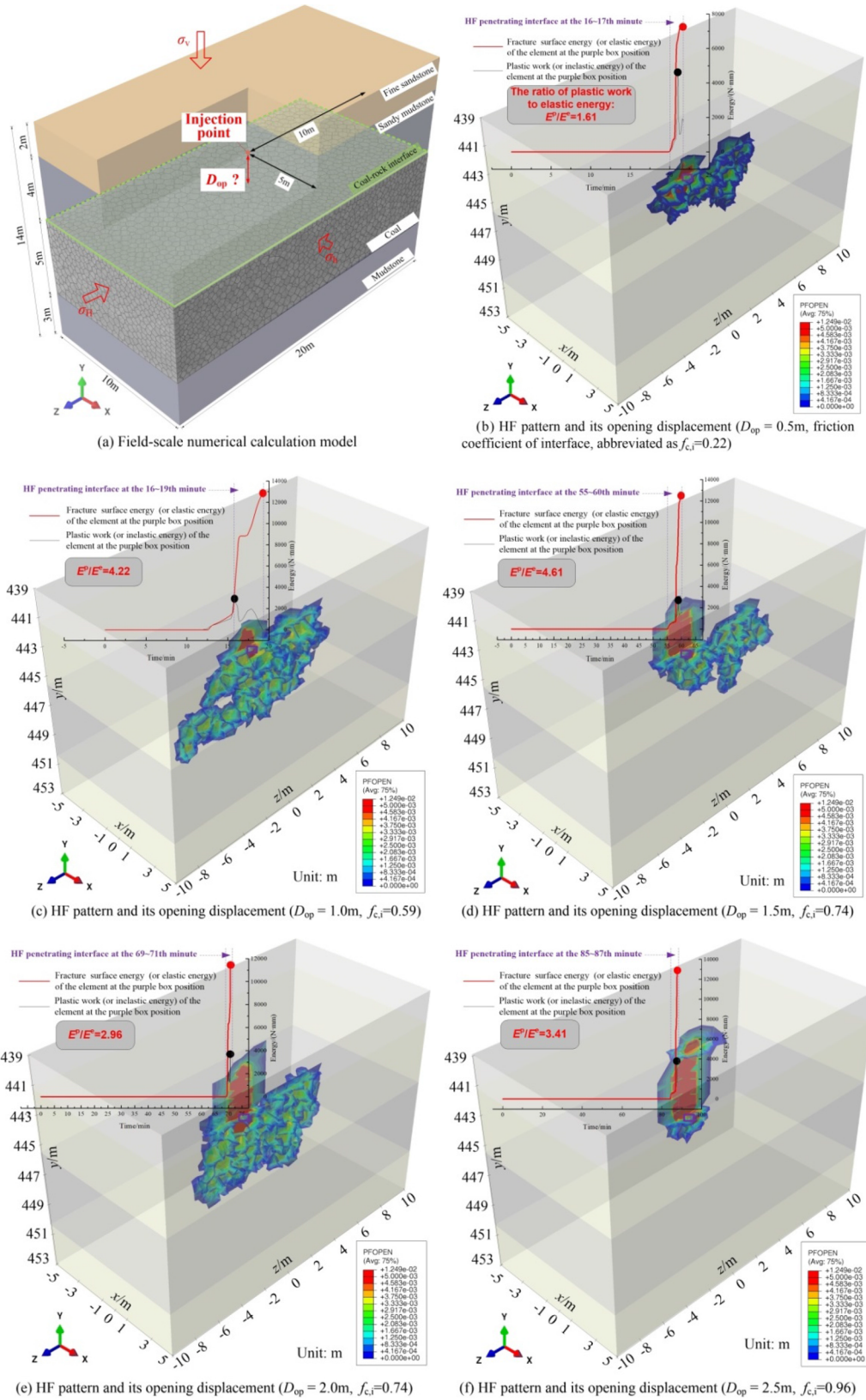
The basic method to obtain the field-scale criterion of HFs crossing coal–rock interface is the control variable method. The specific steps are as follows: (1) controlled $D_{op} = 0.5$ m, and σ_H, σ_h in each stratum (Fig. 2), set $\sigma_v = 13.7$ MPa (differential stress $\Delta\sigma = \sigma_v - \sigma_h = 4$ MPa), then changed the parameters of interface, until HFs crossed the interface;

(2) repeated the step (1), but set $\sigma_v = 14.7$, 15.7, 16.7 and 17.7 MPa ($\Delta\sigma = 5$, 6, 7, 8 MPa), so as to obtain the critical interface parameters for HFs crossing the interface when $D_{op} = 0.5$ m; (3) repeated steps (1) and (2) and set $D_{op} = 1.0$, 1.5, 2.0 and 2.5 m respectively. According to the above steps, 115 numerical models were established to study the field-scale criterion of HFs crossing coal–rock interface under different combinations of the three factors, including D_{op}, $\Delta\sigma$ and interfacial friction coefficient $f_{c,i}$. Because the numerical results are quite a lot, only the case of $\Delta\sigma = 4$, 6, 8 MPa and HFs successfully crossing interface are shown in Fig. 13. And the results under the other conditions are summarized as the field-scale criterion of HFs crossing the interface, as shown in Fig. 14.

Figure 13 shows the results of the HFs opening displacement under the three factors, including $\Delta\sigma = 4-8$ MPa, $D_{op} = 0.5-2.5$ m, and $f_{c,i} = 0.022-0.96$. Compared with results of $D_{op} = 2.0-2.5$ m, the HFs pattern is more complex when $D_{op} = 0.5-1.5$ m. The upper left corner of each picture in Fig. 13 shows the evolution of the plastic work (or inelastic energy) and fracture surface energy (or elastic energy) of the coal elements in purple box. Obviously, when HFs cross the interface, the plastic work and elastic energy will increase rapidly, and the former (red dot in Fig. 13) is usually 0.72–5.15 times of the latter (black dot in Fig. 13), and the larger D_{op} is, the closer the value is to the upper limit. These rule shows that most of the hydraulic energy is consumed on plastic work that does not help HFs propagate, leading to the failure of indirect fracturing technology.
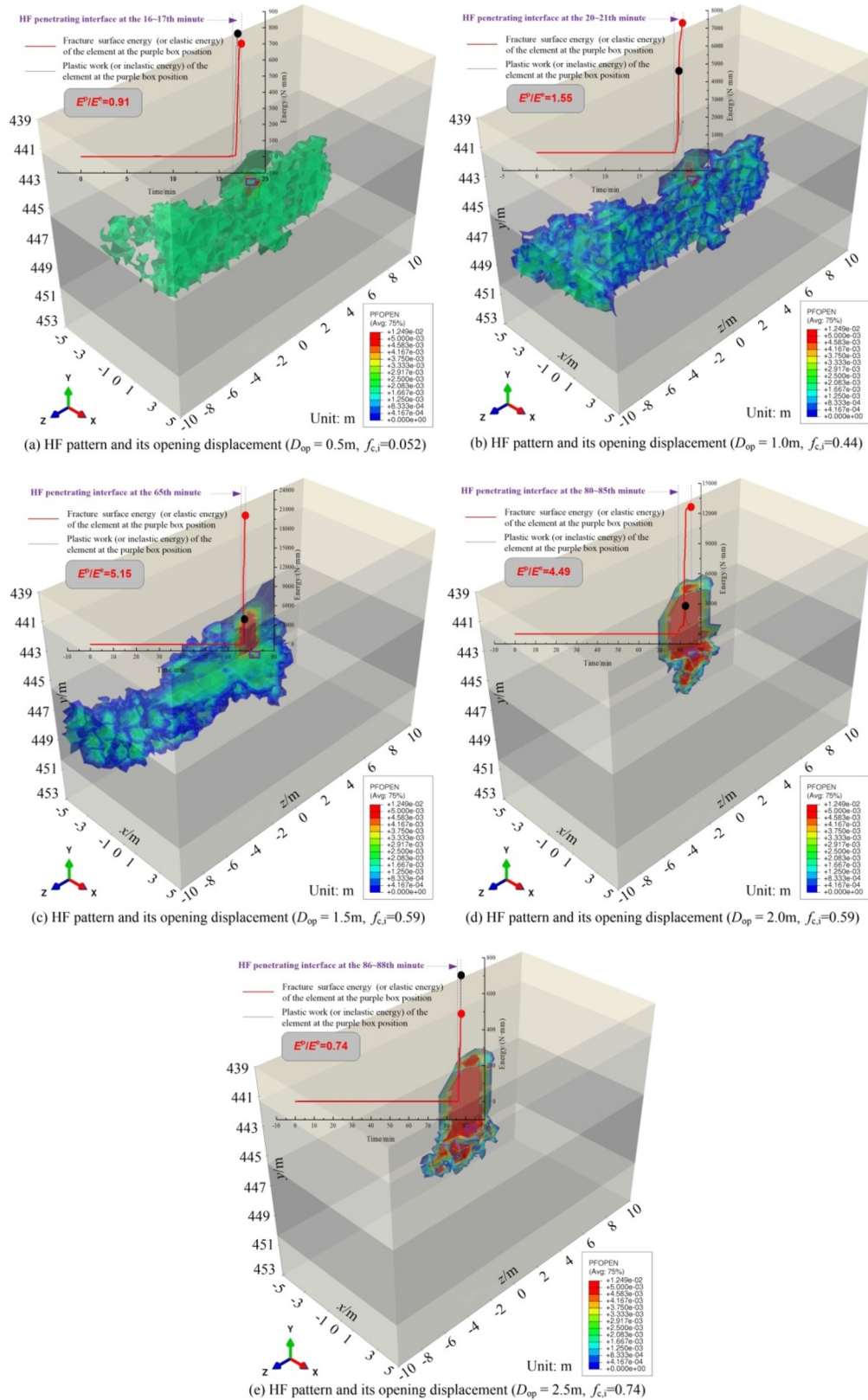
In addition, according to the numerical simulation results, the field-scale criterion of HFs crossing the interface can be obtained, as shown in Fig. 14. Generally speaking, when $\Delta\sigma$ is constant, the critical value of $f_{c,i}$ increases with the increase of D_{op}; when D_{op} is constant, the critical value of $f_{c,i}$ decreases with the increase of $\Delta\sigma$. In other words, under the condition of high in-situ stress difference and horizontal well close to coal rock interface, HFs can cross the coal–rock interface under low interfacial shear strength. The power function was used to fit the data in Fig. 14, the fitting surface (cyan surface in Fig. 14) and the field-scale criterion expressed by inequality can be obtained.

$$\begin{cases} 0.689 - 0.569 D_{op}^{-0.536} + 3.515\Delta\sigma^{-1.162} - 1.238 D_{op}^{-0.536} \cdot \Delta\sigma^{-1.162} - f_{c,i} > 0 \\ \text{Crossing interface} \\ 0.689 - 0.569 D_{op}^{-0.536} + 3.515\Delta\sigma^{-1.162} - 1.238 D_{op}^{-0.536} \cdot \Delta\sigma^{-1.162} - f_{c,i} < 0 \\ \text{Non} - \text{crossing interface} \end{cases} \tag{19}$$
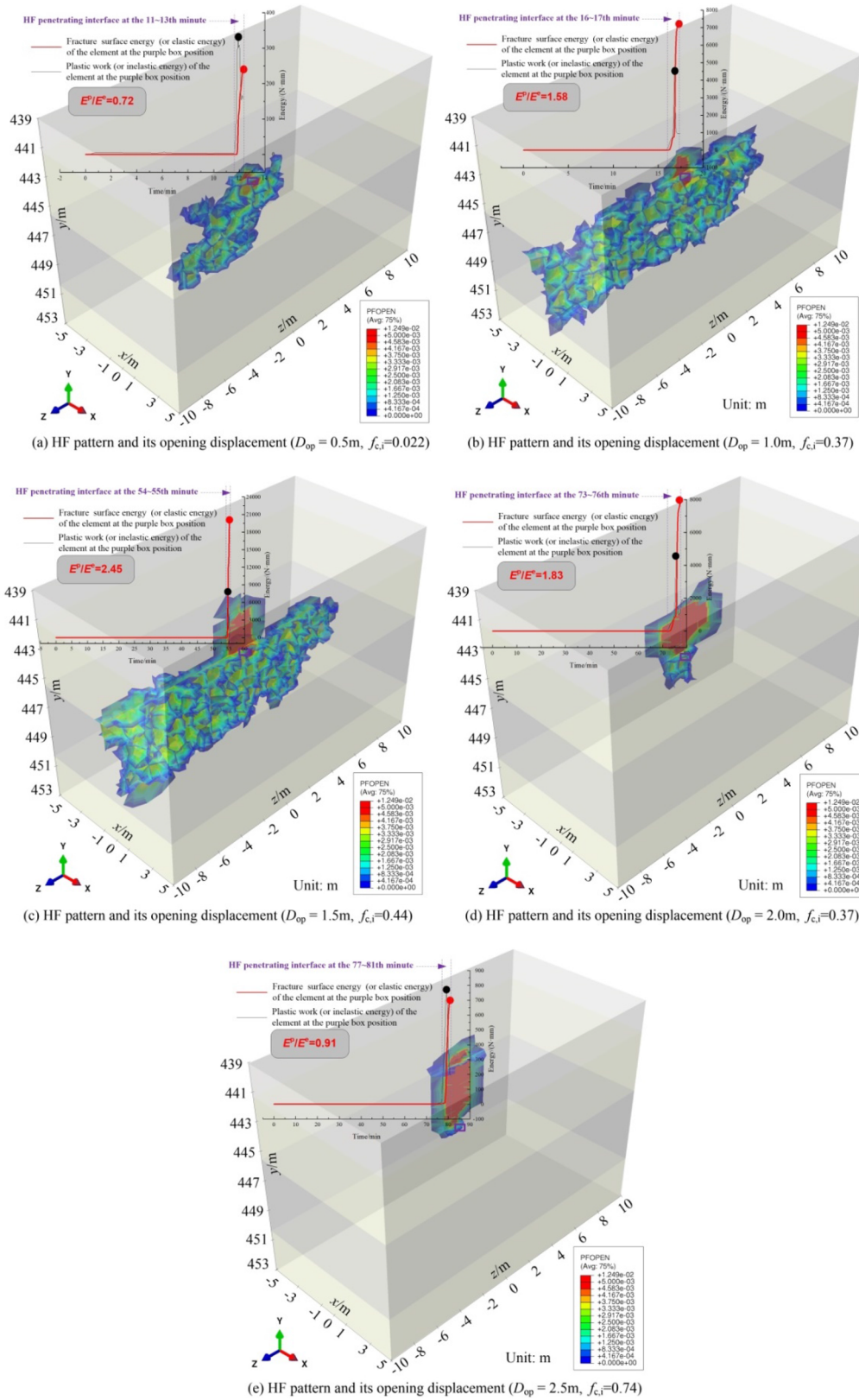
(a) Field-scale numerical calculation model

(b) HF pattern and its opening displacement (D_{op} = 0.5m, friction coefficient of interface, abbreviated as $f_{c,i}$=0.22)

(c) HF pattern and its opening displacement (D_{op} = 1.0m, $f_{c,i}$=0.59)

(d) HF pattern and its opening displacement (D_{op} = 1.5m, $f_{c,i}$=0.74)

(e) HF pattern and its opening displacement (D_{op} = 2.0m, $f_{c,i}$=0.74)

(f) HF pattern and its opening displacement (D_{op} = 2.5m, $f_{c,i}$=0.96)

(I) Hydraulic fracture pattern variations with different D_{op} ($\Delta\sigma$ = 4 MPa)

Fig. 13 Field-scale numerical simulation results of hydraulic fracturing

(a) HF pattern and its opening displacement (D_{op} = 0.5m, $f_{c,i}$=0.052)

(b) HF pattern and its opening displacement (D_{op} = 1.0m, $f_{c,i}$=0.44)

(c) HF pattern and its opening displacement (D_{op} = 1.5m, $f_{c,i}$=0.59)

(d) HF pattern and its opening displacement (D_{op} = 2.0m, $f_{c,i}$=0.59)

(e) HF pattern and its opening displacement (D_{op} = 2.5m, $f_{c,i}$=0.74)

(II) Hydraulic fracture pattern variations with different D_{op} ($\Delta\sigma$ = 6 MPa)

Fig. 13 (continued)

(a) HF pattern and its opening displacement (D_{op} = 0.5m, $f_{c,i}$=0.022)

(b) HF pattern and its opening displacement (D_{op} = 1.0m, $f_{c,i}$=0.37)

(c) HF pattern and its opening displacement (D_{op} = 1.5m, $f_{c,i}$=0.44)

(d) HF pattern and its opening displacement (D_{op} = 2.0m, $f_{c,i}$=0.37)

(e) HF pattern and its opening displacement (D_{op} = 2.5m, $f_{c,i}$=0.74)

(III) Hydraulic fracture pattern variations with different D_{op} ($\Delta\sigma$ = 8 MPa)

Fig. 13 (continued)

It should be noted that expression 19 is only applicable to field-scales of 4 MPa $\leq \Delta\sigma \leq$ 8 MPa and 0.5 m $\leq D_{op} \leq$ 2.5 m. Although this range is relatively narrow, it is enough to guide the application of indirect fracturing coal technology in Zhaozhuang mine.

Based on "field-scale criterion", the effect of HFs crossing coal–rock interface can be improved by the following three methods in engineering practice: reducing D_{op} to less than 1.5 m, maintaining high hydraulic energy (injection rate is 8m^3/min), optimizing the landing of the horizontal well (red line in Fig. 1) so that $\Delta\sigma$ is greater than 6 MPa, meanwhile, the coal near the interface is not too broken to ensure a high $f_{c,i}$ value. Thus, the indirect fracturing coal technology has been successfully applied in Zhaozhuang mine, and the daily production of CBM is 10 times higher than that without parameter optimization, exceeding 3000m^3/day (Fig. 15), which declares the effectiveness of the field-scale criterion (Fig. 14) of HFs crossing the interface between roof and broken low-permeability coal.

6 Discussions

In the present study, we established a 3D discontinuities network model and PF-S constitutive equations for broken soft and low-permeability coal. On this basis, we investigated the field-scale criterion of hydraulic fracture crossing the coal–rock interface under the influence of three factors, including stress difference ($\Delta\sigma$), interface friction coefficient ($f_{c,i}$), and the distance between horizontal well and

coal rock interface (D_{op}). According to the above "criterion", the landing of the horizontal well and process parameters were optimized, and the indirect fracturing coal technology was successfully applied in Zhaozhuang mine. Our research demonstrates that the critical $f_{c,i}$ decreases with the increase of the $\Delta\sigma$ and the decrease of D_{op} when the HFs crossing coal–rock interface, and the critical $f_{c,i}$ is more significantly affected by the D_{op} than the $\Delta\sigma$. Compared with the lab-scale criterion (Jiang et al. 2019; Wang et al. 2018), this finding is significant because the field-scale criterion offers an upper limit of D_{op} in engineering practice, specifically, the HFs in the roof will be greatly hindered by the interface once the D_{op} exceeds 2 m (Figs. 13Ie, f, 13IId, e, 13IIId, e). Currently, two core issues determining the adequacy of numerical simulation results, that is, PF-S constitutive equations and 3D discontinuities network model for the broken soft and low-permeability coal, have been established and verified by CT experiments, fracture mechanics tests and HF experiments respectively. To our knowledge, it is the first time to study the effect of D_{op} on field-scale criterion by combining PF-S constitutive equations and 3D discontinuities network model.

As is known, broken soft coal have significant nonlinear mechanical characteristics, which will cause hydraulic energy to be mainly used for consuming plastic work rather than the fractures surface energy during HFs propagation process, resulting in short HFs length and low CBM production. Linear elastic fracture mechanics theory (Llanos et al. 2017), elastic damage mechanics theory (Guo et al. 2017), and traditional fluid–solid coupling theory (Kanaun 2018) based on ECM (Hao et al. 2013) or DCM models (Moinfar et al. 2013) were widely used to predict HFs propagation in brittle layered rocks with a few of discontinuities. However, for the broken soft and low-permeability coal in Zhaozhuang mine, the field-scale criterion cannot be derived
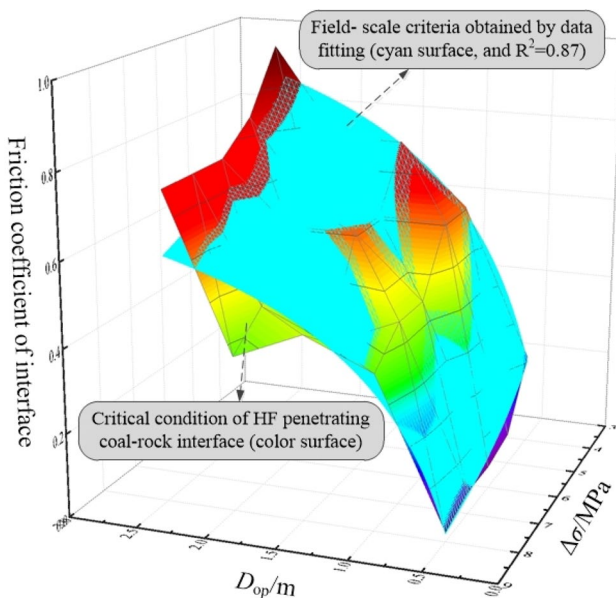

Fig. 14 The field-scale criterion of hydraulic fracture crossing the interface between roof and broken low-permeability coal
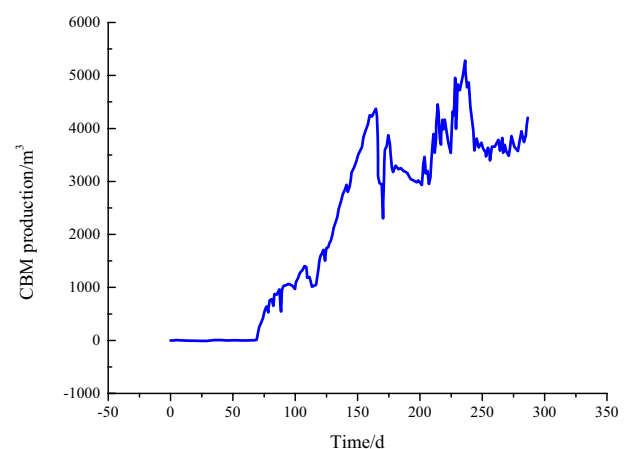

Fig. 15 In-situ test results of daily production of CBM by indirect fracturing technology

from these theories, because they were conducted lack of the influence of the interaction between nonlinear fracture of discontinuities and inelastic deformation of coal matrix (Eqs. 4, 12 and Fig. 7), lack of the influence of the nonlinear response on seepage (Eqs. 9, 18), and lack of consideration of discontinuities network geometric characteristics of broken soft coal (Fig. 4). The criterion of hydraulic fracture crossing coal–rock interface obtained by elastic mechanics theory are unreliable. As shown in Fig. 16a, b (or 12Ia) and Fig. 16c, the results of numerical simulation based on PF-S constitutive equations are similar to the experimental results, but based on the elastic theory, HFs can cross the coal–rock interface. In addition, it is limited to explain the mechanism of hydraulic energy loss during the propagation of HFs in broken soft coal by damage mechanics theory. For brittle or quasi-brittle rock masses such as shale and dry hot granite, the failure mechanism is mainly the expansion of micro-cracks, which can be described by the damage mechanics theory in macroscopic view. While for the broken soft coal, it has the characteristics of low elastic modulus, high Poisson's ratio, and significant ductility properties. Its failure mechanism includes two aspects: the expansion of micro-cracks and the plastic deformation of the coal matrix. However, damage mechanics can only describe the energy loss caused by "micro-crack expansion", but cannot reflect the energy loss caused by the plastic deformation. This will cause the elastic energy (or fracture surface energy) obtained by the damage mechanics model to be larger than the value obtained by the PF-S in this article, because the consumption of hydraulic energy by plastic work is neglected. As a result, HFs are easier to cross the coal–rock interface obtained by the damage mechanics theory, which may lead to failure of indirect fracturing engineering practice. In terms of seepage behavior, the tangential flow of fracturing fluid in coal discontinuities and the leak-off of fracturing fluid (normal flow) are considered in this article. The tangential flow is described by the cubic law, although it is simple, it can reflect the main characteristics of the seepage in discontinuities with low computational cost. For normal flow (or leak-off behavior of fracturing fluid), it is mainly affected by the plastic damage of coal matrix, which will lead to the obvious change of permeability coefficient, k_{nd}. The parameter k_{nd} can be obtained by permeability test in the whole stress–strain process. Thus, the permeability characteristics of low-permeability coal can be obtained. The adequacy of PF-S constitutive equations can be verified by laboratory tests (Figs. 8, 9, 10, 15), makes the results more meaningful.

To date, most researchers have simplified the discontinuities network geometry of the coal into 2D form based on the "ECM or DCM method" (Zhao et al. 2020; Zhuang et al. 2020). These 2D geometric models can partly explain the changes of stress, displacement and water pressure in the plane during HFs propagation. However, the reason for HFs crossing the interface is that the 3D discontinuities in coal and rock are connected under the action of water pressure and 3D stress, and it seems a bit far-fetched to obtain the criterion directly from 2D model. As shown in Fig. 12Ia, HFs can cross the coal–rock interface when $\Delta\sigma = 6$ MPa in the 3D model, while in 2D model (Fig. 17), the same situation only occurs when $\Delta\sigma = 10$ MPa, which indicates that the "criterion" obtained by 2D model is unreliable. Although cleat network based on and 3D DFN method was proposed in some previous studies (Lan and Gong, 2020; Yu et al. 2016, as shown in Fig. 18), it is still unclear whether they can be applied to the broken soft coal because these geometry models were proposed for primary structure coal.

In this study, we established a 3D discontinuities network model for broken soft coal based on CT experiment (Fig. 4),
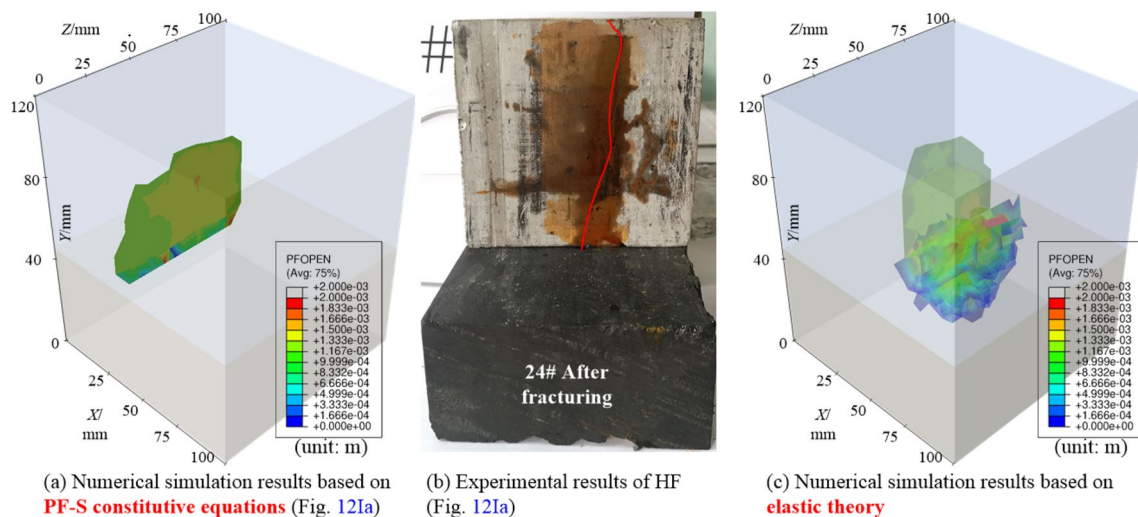

(a) Numerical simulation results based on PF-S constitutive equations (Fig. 12Ia)

(b) Experimental results of HF (Fig. 12Ia)

(c) Numerical simulation results based on elastic theory

Fig. 16 Comparison of numerical simulation results based on elastic and PF-S constitutive equations

and the PF-S constitutive equations were proposed on the basis of comprehensive analysis of coal matrix plasticity, nonlinear fracture of coal discontinuity and their influence on seepage. These models and equations lay the foundation for establishing the field-scale criterion of hydraulic fracture crossing the coal–rock interface (Expression 19, Fig. 14), and provide a theoretical support for improving the CBM production in areas of broken soft and low-permeability coal by indirect fracturing technology (Fig. 19).

7 Conclusions

This article closely focuses on the PF-S constitutive equations and 3D discontinuities network model of the broken soft and low-permeability coal, and then studies the field-scale criterion of HFs crossing coal–rock interface. The results provides a theoretical basis for employing indirect fracturing technology to increase CBM production in areas of broken soft and low—permeability coal. The main conclusions are summarized as follows:

1. The 3D discontinuities network model based on CT experiment can well reflect the discontinuities network geometry of broken soft and low-permeability coal, and PF-S constitutive equations based on nonlinear mechanics-seepage theory can reflect the interaction among nonlinear fracture mechanics of the coal discontinuities, plastic mechanics of coal matrix and seepage characteristics of matrix and discontinuities.

2. The field-scale criterion of hydraulic fracture crossing coal–rock interface shows that the critical $f_{c,i}$ is positively correlated with D_{op} and negatively correlated with $\Delta\sigma$, and it is more affected by D_{op}. The critical $f_{c,i}$ will increase rapidly once D_{op} is greater than 2 m, making it difficult for HFs crossing the coal–rock interface.
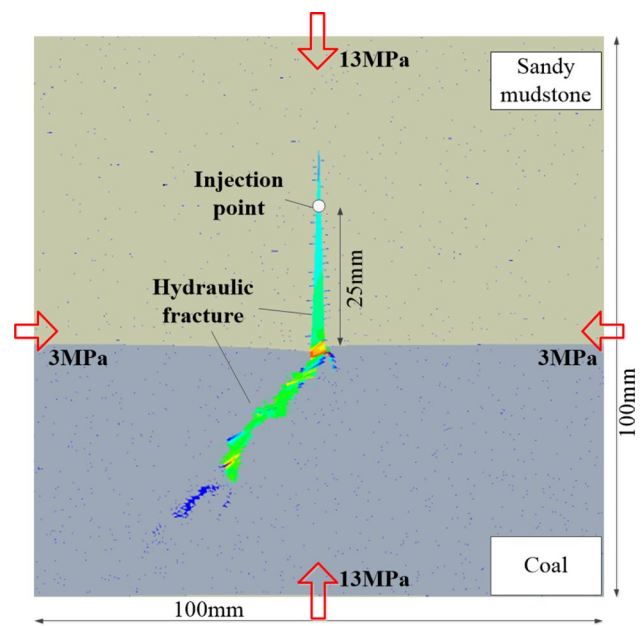

Fig. 17 HF Numerical results obtained from plane strain model (HF penetrates coal–rock interface when $\Delta\sigma = 10$ MPa)

3. The coal discontinuities will lead HFs to form a more energy-consuming mixed fracture mode, coupled with the significant inelastic deformation characteristics, resulting in the loss of hydraulic energy as high as 42–84% ($0.5 \text{ m} \leq D_{op} \leq 2.0 \text{ m}$) during the process of HF crossing the interface. And with the increase of D_{op}, the hydraulic energy loss tends to approach the upper limit. This is the main reason that HFs are difficult to cross coal–rock interface.

4. Based on "field-scale criterion", by optimizing the landing of the horizontal well (i.e. increasing $\Delta\sigma$), reducing D_{op} and maintaining a high hydraulic energy input, the success rate of indirect fracturing coal technology in

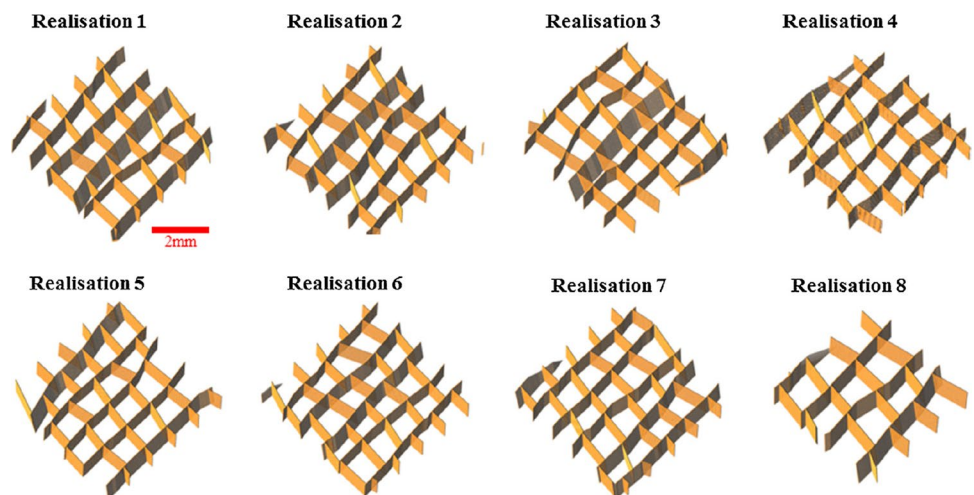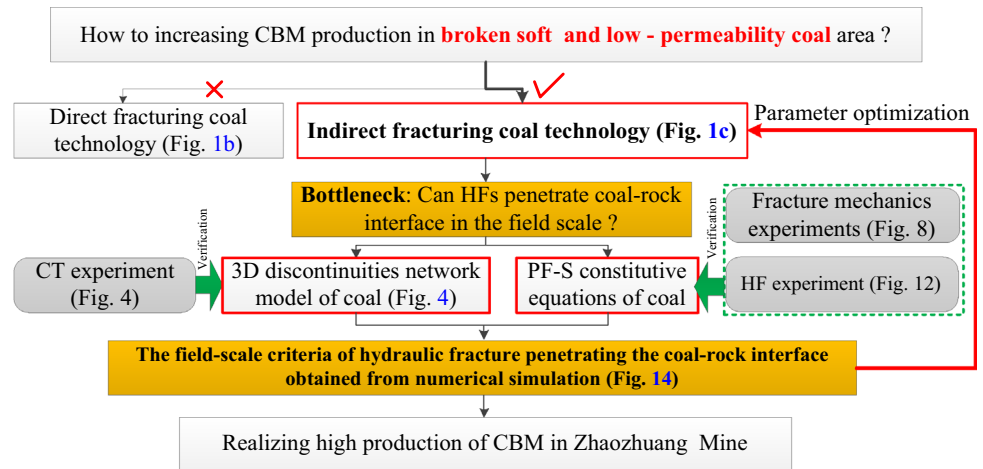**Fig. 18** Cleat network geometry model of primary structure coal (Yu et al. 2016)

Fig. 19 Steps for realizing high production of CBM in broken low-permeability coal area using field-scale criterion of hydraulic fracture crossing coal–rock interface

areas of broken soft and low-permeability coal can be greatly increased.

References

Afsar F, Philipp SL, Westphal H (2011) Fracture propagation and reservoir permeability in limestone-marl alternations of the Jurassic Blue Lias Formation (Bristol Channel Basin, UK): a multidisciplinary approach. Geophysical Research Abatracts.

Aimene Y, Hammerquist C, Ouenes A (2019) Anisotropic damage mechanics for asymmetric hydraulic fracture height propagation in a layered unconventional gas reservoir. J Nat Gas Sci Eng 67:1–13

Athavale AS, Miskimins JL (2008) Laboratory hydraulic fracturing tests on small homogeneous and laminated blocks. U.S. Rock Mechanics Symposium

Dehghan AN, Goshtasbi K, Ahangari K et al (2015) The effect of natural fracture dip and strike on hydraulic fracture propagation. Int J Rock Mech Min Sci 75:210–215

Detournay E (2016) Mechanics of hydraulic fractures. Annu Rev Fluid Mech 48:311–339

Fei K, Zhang JW (2013) Application of ABAQUS in geotechnical engineering. China Water & Power Press, Beijing (**in Chinese**)

Guo JC, Luo B, Lu C et al (2017) Numerical investigation of hydraulic fracture propagation in a layered reservoir using the cohesive zone method. Eng Fract Mech 186:195–207

Hao Y, Fu P, Carrigan CR (2013) Application of a dual-continuum model for simulation of fluid flow and heat transfer in fractured geothermal reservoirs. In: The 38th Stanford Geothermal Workshop.

He KK (2018) Characterization of multiscale pores and fissures in coal based on CT scan. Dissertation, Henan Polytechnic University (in Chinese)

Huang S, Liu D, Cai Y et al (2019) In situ stress distribution and its impact on CBM reservoir properties in the Zhengzhuang area, southern Qinshui Basin, North China. J Nat Gas Sci Eng 61:83–96

Huang SP, Liu DM, Yao YB et al (2017) Natural fractures initiation and fracture type prediction in coal reservoir under different in-situ stresses during hydraulic fracturing. J Nat Gas Sci Eng 43:69–80

Izadia G, Wang SG, Elsworth D et al (2011) Permeability evolution of fluid-infiltrated coal containing discrete fractures. Int J Coal Geol 85(2):202–211

Jiang TT, Zhang JH, Hao Wu (2016) Experimental and numerical study on hydraulic fracture propagation in coalbed methane reservoir. J Nat Gas Sci Eng 35:155–467

Jiang YL, Lian HJ, Nguyen VP, et al (2019) Propagation behavior of hydraulic fracture across the coal-rock interface under different interfacial friction coefficients and a new prediction model. J Nat Gas Sci Eng 68: 102894.

Kanaun S (2018) Efficient numerical solution of the hydraulic fracture problem for planar cracks. Int J Eng Sci 127:114–126

Karimpouli S, Tahmasebi P, Ramandi HL et al (2017) Stochastic modeling of coal fracture network by direct use of microcomputed tomography images. Int J Coal Geol 179:153–163

Keshavarz A, Badalyan A, Johnson R Jr et al (2016) Productivity enhancement by stimulation of natural fractures around a hydraulic fracture using micro-sized proppant placement. J Nat Gas Sci Eng 33:1010–1024

Kim CM, Abass HH (1991) Hydraulic fracture initiation from horizontal wellbores: laboratory Experiments. In: Symposium on Rock Mechanics 10–12 July, Norman

Lan ZK, Gong B (2020) Uncertainty analysis of key factors affecting fracture height based on box-behnken method. Eng Fract Mech 228:106902

Li SY, He TM, Yin XC (2015) Rock fracture mechanics. Science Press, Beijing (**in Chinese**)

Li LC, Tang CA, Liang ZZ et al (2009) Numerical simulation on water inrush process due to activation of collapse columns in coal seam floor. J Min Saf Eng 26(2):158–162

Liu Y, Wang D, Hao F et al (2017) Constitutive model for methane desorption and diffusion based on pore structure differences between soft and hard coal. Int J Min Sci Technol 27(6):937–944

Liu YB, Li MH, Yin GZ et al (2018) Permeability evolution of anthracite coal considering true triaxial stress conditions and structural anisotropy. J Nat Gas Sci Eng 52:492–506

Llanos EM, Jeffrey RG, Hillis R et al (2017) Hydraulic fracture propagation through an orthogonal discontinuity: a laboratory, analytical and numerical study. Rock Mech Rock Eng 50:2101–2118

Ma Q, Harpalani S, Liu SM (2011) A simplified permeability model for coalbed methane reservoirs based on matchstick strain and constant volume theory. Int J Coal Geol 85:43–48

Moinfar A, Varavei A, Sepehrnoori K et al. (2013) Development of a coupled dual continuum and discrete fracture model for the simulation of unconventional reservoirs. In: SPE Reservoir Simulation Symposium. Society of Petroleum Engineers.

Olsen TN, Bratton TR, Donald A et al (2007) Application of indirect fracture for efficient stimulation of coalbed methane. In: SPE Rocky Mountain Oil & Gas Technology Symposium. Denver, Colorado. 16–18. April, pp. 1–10.

Ortiz M, Pandolfi A (2018) Finite-deformation irreversible cohesive elements for three-dimensional crack-propagation analysis. Int J Numer Meth Eng 44(9):1267–1282

Park K, Paulino GH, Roesler JR (2008) Virtual internal pair-bond model for quasi-brittle materials. J Eng Mech 134(10):856–866

Poludasu S, Awoleke O, Ahmadi M et al (2016) Using experimental design and response surface methodology to model induced fracture geometry in Shublik shale. J Unconv Oil and Gas Resour 15:43–55

Sakhaee-Pour A, Wheeler MF (2016) Effective flow properties for cells containing fractures of arbitrary geometry. SPE J 21:0965–0980

Sampath K, Perera MSA, Ranjith PG et al (2017) CH_4CO_2 gas exchange and supercritical CO_2 based hydraulic fracturing as CBM production-accelerating techniques: A review. J CO2 Util 22:212–230

Shi JQ, Durucan S (2004) Drawdown induced changes in permeability of coalbeds: a new interpretation of the reservoir response to primary recovery. Transp Porous Media 56:1–16

Shi Z (2019) Study on simulation method of meso-cracking of asphalt concrete. Dissertation, Hunan University of Science and Technology (in Chinese)

Tan P, Jin Y, Han K et al (2017) Vertical propagation behavior of hydraulic fractures in coal measure strata based on true triaxial experiment. J Pet Sci Eng 158:398–407

Thakur P (2017) Global reserves of coal bed methane and prominent coal basins. Adv Reserv Prod Eng for Coal Bed Methane 2017:1–15

Vahab M, Akhondzadeh Sh, Khoei AR et al (2018) An X-FEM investigation of hydro-fracture evolution in naturally-layered domains. Eng Fract Mech 191:187–204

Wang EY, Yi WX, Li YB (2015) Distribution and genetic mechanism of tectonic coal in North China. Science Press, BeiJing ((**in Chinese**))

Wang T, Liu ZL, Gao Y (2018) A prediction criterion for the interaction between hydraulic fractures and natural fractures based on given parameters. Eng Mech 35(11):216–222

Yang JF (2019) Study on the constitutive equation of the cohesive crack in coals and its application in fracturing engineering. Dissertation, Taiyuan University of Technology (in Chinese)

Yu J, Ryan TA, Hamed LR et al (2019) DigiCoal: A computational package for characterisation of coal cores. J Petrol Sci Eng 176:775–791

Yu J, Ryan TA, Hamed LR et al (2016) Coal cleat reconstruction using micro-computed tomography imaging. Fuel 181:286–299

Zhang J, Liu D, Cai Y et al (2017) Geological and hydrological controls on the accumulation of coalbed methane within the No. 3 coal seam of the southern Qinshui Basin. Int J Coal Geol 182:94–111

Zhang Q, GeLi CGW et al (2018) A new model and application of coalbed methane high efficiency production from broken soft and low permeable coal seam by roof strata-in horizontal well and staged hydraulic fracture. J China Coal Soc 43(1):150–159

Zhao JJ, Zhang Y, Ranjithc PG (2020) Numerical modelling of blast-induced fractures in coal masses under high in-situ stresses. Eng Fract Mech 225:106749